

Low-temperature phases of interacting bosons in a lattice

Akshay Shankar

A dissertation submitted for the partial fulfilment of BS-MS dual degree in Science



Indian Institute of Science Education and Research, Mohali

10th April 2023

Certificate of Examination

This is to certify that the dissertation titled **Low-temperature phases of interacting bosons in a lattice** submitted by **Akshay Shankar** (Reg. No. MS18117) for the partial fulfillment of BS- MS Dual Degree programme of the institute, has been examined by the thesis committee duly appointed by the institute. The committee finds the work done by the candidate satisfactory and recommends that the report be accepted.

Prof. Dr. Tilman Pfau

Prof. Yogesh Singh

Prof. Abhishek Chaudhuri

Prof. Sanjeev Kumar
(Supervisor)

Dated: 10th April 2023

Declaration

The work presented in this dissertation has been carried out by me under the guidance of Prof. Sanjeev Kumar at the Indian Institute of Science Education and Research, Mohali.

This work has not been submitted in part or in full for a degree, a diploma, or a fellowship to any other university or institute. Whenever contributions of others are involved, every effort is made to indicate this clearly, with due acknowledgement of collaborative research and discussions. This thesis is a bonafide record of original work done by me and all sources listed within have been detailed in the bibliography.

Akshay Shankar

(Candidate)

Dated: 10th April, 2023

In my capacity as the supervisor of the candidates project work, I certify that the above statements by the candidate are true to the best of my knowledge.

Prof. Sanjeev Kumar

(Supervisor)

Dated: 10th April, 2023

Acknowledgements

Use this section to acknowledge the help/contribution of others.

Abstract

Use this section to include an abstract of the thesis.

Contents

Abstract

1	Introduction	1
1.1	Analog Quantum Simulation	1
1.2	Optical Lattices	1
1.3	Outline of the thesis	1
2	Quantum mechanics of periodic lattices	2
2.1	Exploiting structure	2
2.2	Constructing a localized basis	7
3	The Bose-Hubbard model	9
3.1	Derivation	9
3.2	Ground state phases	10
3.3	Connecting theory and experiment	12
4	Solving the Bose-Hubbard model	14
4.1	Exact Diagonalization	14
4.2	Mean Field Theory	17
4.3	Cluster Mean Field Theory	25
5	Dipolar bosons in a lattice	28
5.1	Mean Field Theory	28
5.2	Analysis	29
5.3	Caveats w/ self-consistency	33
6	Spinful bosons in a lattice	36
6.1	Mean Field Theory	36
6.2	Results	39
6.3	Effective spin-spin interactions	41
7	Boson-mediated interactions	43
7.1	Strong-coupling limit	43

8	Going beyond the Mean Field	46
8.1	Variational Monte Carlo	46
8.2	Stochastic Series Expansion	48
Appendix A	Setting up MFT numerically	57
Appendix B	Diagonalizing spin interactions	58
Appendix C	Degenerate first order perturbation theory	59

CHAPTER

1

Quantum mechanics of periodic lattices

In this chapter, we will review the basic concepts of the physics of a particle trapped in a periodic potential. This will set the stage for extending our formalism to the many-particle system of bosons that we wish to study in this thesis.

1.1 Exploiting structure

Consider a particle of mass m trapped in a 1D periodic potential $V(x)$ with period a . The hamiltonian can then be written as:

$$\hat{H} = \frac{\hat{p}^2}{2m} + \hat{V}(x) \quad V(x+a) = V(x) \quad (1.1)$$

In an attempt to uncover some structure in this system, let us draw a parallel with the special case of a free-particle where $V(x) = 0$. Such a system has a continuous translation symmetry, i.e, $V(x+a) = V(x) \forall a$. As a result of Noether's theorem, the momentum k is a conserved quantity and hence a good quantum number to label the eigenstates.

However, in the case of a periodic potential, the system only has a discrete translation symmetry. Equivalently, the hamiltonian remains invariant under the action of the translation operator, $\hat{T}_a = e^{-i\hat{p}a/\hbar}$:

$$\hat{T}_a \hat{H} \hat{T}_a^{-1} = \hat{H} \quad \iff \quad [\hat{T}_a, \hat{H}] = 0 \quad (1.2)$$

We can then find the common eigenbasis of \hat{H} and \hat{T}_a :

$$\hat{H}\psi_{E,\alpha}(x) = E\psi_{E,\alpha}(x) \quad \hat{T}_a\psi_{E,\alpha}(x) = \psi_{E,\alpha}(x+a) = e^{i\alpha}\psi_{E,\alpha} \quad (1.3)$$

where the eigenvalues of \hat{T}_a must be pure phases since it is a unitary operator. Now consider the following function $u_{E,\alpha}(x) = e^{-iqx}\psi_{E,\alpha}(x)$ and its behaviour under the action of \hat{T}_a :

$$\begin{aligned} \hat{T}_a u_{E,\alpha}(x) &= \hat{T}_a e^{-iqx} \psi_{E,\alpha}(x) \\ &= e^{-iq(x+a)} \psi_{E,\alpha}(x+a) \\ &= e^{-iqa} e^{i\alpha} e^{-iqx} \psi_{E,\alpha}(x) \\ u_{E,\alpha}(x+a) &= e^{i(\alpha-q\alpha)} u_{E,\alpha}(x) \end{aligned}$$

If we choose to set $\alpha = qa$, $u_{E,\alpha}(x)$ becomes periodic with respect to x ! Substituting this relation and flipping the definition of $u(x)$ gives us the following result.

$$\psi_{E,q}(x) = e^{iqx} u_{E,q}(x) \quad u_{E,q}(x+a) = u_{E,q}(x) \quad (1.4)$$

This is simply a statement of Bloch's theorem, where $\psi_{E,q}$ are the bloch wave-functions and q is the quasi-momentum. It can be easily seen that $\psi_{E,q}$ is invariant under $q \rightarrow q + 2\pi/a$. This is a manifestation of the fact that q belongs to the reciprocal lattice of the system, and it is sufficient to work with the values of q within a single unit cell. Generally, this is chosen to be the Wigner-Seitz cell of the reciprocal lattice, i.e, the first brillouin zone where $q \in [-\frac{\pi}{a}, \frac{\pi}{a}]$.

Applying the time-independant schrodinger equation to the bloch wave-function, we get:

$$\hat{H}_q u_q^n(x) = \left[\frac{\hbar^2}{2m} \left(-i \frac{d}{dx} + q \right)^2 + V(x) \right] u_q^n(x) = E_q^n u_q^n(x) \quad (1.5)$$

where we have replaced E with the band index n . This can now be solved to obtain the energy bands and eigenstates of the system.

1.1.1 Bloch wave-functions

We will proceed to study this system by numerically diagonalizing the hamiltonian. Let us consider the specific case of $V(x) = V_0 \cos^2(kx)$ such that $V(x+a) = V(x)$ where $a = \pi/k$. In order to simplify the analysis, we begin by introducing some dimensionless variables $\tilde{x} = x/a$ ($\implies \tilde{q} = \pi q/k$):

$$\hat{H}_q u_q^n(\tilde{x}) = \left[\frac{1}{\pi^2} \frac{\hbar^2 k^2}{2m} \left(-i \frac{d}{d\tilde{x}} + \tilde{q} \right)^2 + V_0 \cos^2(\pi \tilde{x}) \right] u_q^n(\tilde{x}) = E_q^n u_q^n(\tilde{x}) \quad (1.6)$$

As a result of this manipulation, a natural unit of energy has emerged, $E_r = \hbar^2 k^2 / 2m$, which is simply the recoil energy in the context of optical lattices. We can now write the complete dimensionless hamiltonian as follows:

$$\hat{H}_q u_q^n(\tilde{x}) = \left[\frac{1}{\pi^2} \left(-i \frac{d}{d\tilde{x}} + \tilde{q} \right)^2 + \tilde{V}_0 \cos^2(\pi \tilde{x}) \right] u_q^n(\tilde{x}) = \tilde{E}_q^n u_q^n(\tilde{x}) \quad (1.7)$$

We will drop the \sim from the variables hereafter but it is implied that we are working with the corresponding dimensionless quantities. It is now sufficient to solve the system within a single unit cell, such that $x \in [-0.5, 0.5]$ and $q \in [-\pi, \pi]$. We now discuss two possible approaches to solve this eigenvalue problem numerically.

Position basis

As the equation is already written in the position basis, it seems like a natural choice to use it to construct our hamiltonian matrix. We start by discretizing our spatial grid $x \in [x_1, x_N]$ into N equally spaced points like so, $x_k = x_1 + (k - 1)\Delta x$ where $\Delta x = (x_N - x_1)/N$ and $k \in [1, N]$.

The wavefunction is then represented as a vector of values $u_q^n \equiv [u_q^n(x_1), u_q^n(x_2), \dots, u_q^n(x_N)]$ instead of an analytical expression. Similarly, the potential term $V(x)$ is readily seen as a diagonal matrix with the entries $[V(x_1), V(x_2), \dots, V(x_N)]$. The kinetic energy term, however, requires further consideration.

$$\left(-i\frac{d}{dx} + q\right)^2 = -\frac{d^2}{dx^2} - 2iq\frac{d}{dx} + q^2$$

Since our position grid is already discretized, these derivatives can be represented using finite difference schemes like so:

$$\frac{d}{dx}u_q^n(x_k) = \frac{u_q^n(x_{k+1}) - u_q^n(x_{k-1})}{2\Delta x} \quad \frac{d^2}{dx^2}u_q^n(x_k) = \frac{u_q^n(x_{k+1}) - 2u_q^n(x_k) + u_q^n(x_{k-1})}{(\Delta x)^2}$$

This gives us a (nearly) tridiagonal hermitian matrix for the kinetic energy term.

$$\hat{H}_k = \frac{1}{\pi^2} \begin{pmatrix} \alpha & \beta & . & . & . & . & \beta^* \\ \beta^* & \alpha & \beta & . & . & . & . \\ . & \beta^* & \alpha & \beta & . & . & . \\ . & . & \ddots & \ddots & \ddots & . & . \\ . & . & . & \beta^* & \alpha & \beta & . \\ . & . & . & . & \beta^* & \alpha & \beta \\ \beta & . & . & . & . & \beta^* & \alpha \end{pmatrix} \quad \begin{aligned} \alpha &= 2/(\Delta x)^2 + q^2 \\ \beta &= -1/(\Delta x)^2 - iq/\Delta x \end{aligned}$$

The terms at the corners of the matrix enforce the periodic boundary condition due to the derivatives coupling the $k = 0$ and $k = N$ position indices. In the absence of these, the matrix would encode a fixed boundary condition, i.e., $u_q^n(x_0) = u_q^n(x_N) = 0$.

At this point we have completely constructed the hamiltonian matrix, and its eigenvalues can be obtained using standard diagonalization algorithms. However, it turns out that such a scheme is not very efficient and produces significant deviation of the energy bands near the edges of the first brillouin zone. This can be understood by interpreting this procedure as expanding the wavefunction using a set of position basis functions, i.e., a set of dirac deltas, $\delta(x - x_i) \forall i \in [1, N]$. As a result, the co-efficient of such basis elements is simply the value of the wavefunction at that position. This representation is clearly a poor choice for the system since we have not leveraged its periodicity in any way.

Fourier basis

In order to choose a better basis, we note that $V(x)$ and $u_q^n(x)$ have the same periodicity. We can then expand them as a discrete fourier sum using a plane-wave basis.

$$V(x) = \sum_m V_m e^{2\pi i m x} \quad u_q^n(x) = \sum_m c_m^{n,q} e^{2\pi i m x} \quad (1.8)$$

Note that we are still working with the dimensionless variables. Substituting this in Eq. (2.7), we get an expression for the kinetic energy, which is diagonal in this basis:

$$\frac{1}{\pi^2} \left(-i \frac{d}{dx} + q \right)^2 u_q^n(x) = \sum_m \left(2m + \frac{q}{\pi} \right)^2 e^{2\pi i m x} c_m^{n,q} \quad (1.9)$$

Similarly, the potential energy is given by:

$$V(x) u_q^n(x) = \sum_m \sum_{l'} V_m e^{2\pi i (m+l') x} c_{l'}^{n,q} = \sum_m \sum_l V_m e^{2\pi i l x} c_{m-l}^{n,q} \quad (1.10)$$

It is also readily seen that our specific choice of the lattice potential only results in three non-zero coefficients of the fourier sum.

$$V(x) = V_0 \cos^2(\pi x) = \frac{V_0}{4} (e^{2\pi i x} + e^{-2\pi i x} + 2) \quad (1.11)$$

Putting together Eq. (2.9), Eq. (2.10) and Eq. (2.11), we can write the Schrodinger equation as a matrix equation:

$$\sum_{m'} H_{m,m'} \cdot c_{m'}^{n,q} = \epsilon_q^n c_m^{n,q} \quad (1.12)$$

where the matrix form of the hamiltonian is determined as follows:

$$H_{m,m'} = \begin{cases} \left(2m + \frac{q}{\pi} \right)^2 + V_0/2 & \text{if } |m - m'| = 0 \\ V_0/4 & \text{if } |m - m'| = 1 \\ 0 & \text{otherwise} \end{cases} \quad (1.13)$$

Since this basis set implicitly takes the periodicity of the system into account, we do not have to restrict our analysis within a particular unit cell. At this point, the fourier expansion runs over infinite terms, so we will have to truncate it at an arbitrary m_{max} such that $m \in [-m_{max}, m_{max}]$ resulting in a matrix of dimension $(2m_{max} + 1) \times (2m_{max} + 1)$. It turns out that a very small value of m_{max} (~ 10) is sufficient to study the lowest energy bands. In comparison, we required $N \sim 100$ when we used the position basis.

1.1.2 Results

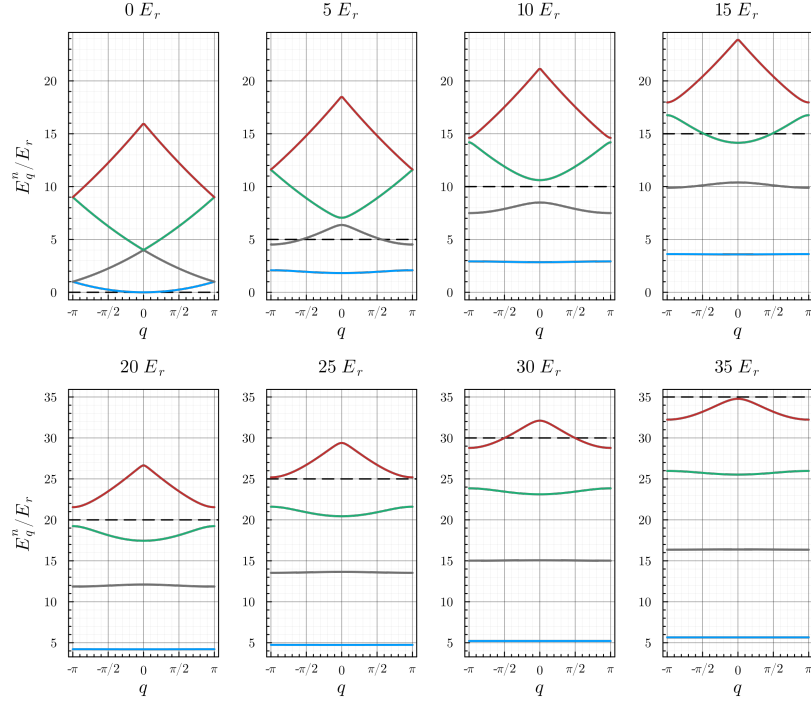


Figure 1.1: First four energy bands of a 1D lattice for various lattice potentials.

In Fig. 2.1 we have plotted the energy bands for the 1D system by diagonalizing the hamiltonian in the fourier basis. We see that for the free particle case ($V = 0$), we have the usual parabolic band structure. However, as the lattice potential is increased, band gaps emerge and the lower band widths become smaller, resulting in equally spaced flat bands. This is expected since we can approximate the minima of the periodic potential as a harmonic oscillator for large V .

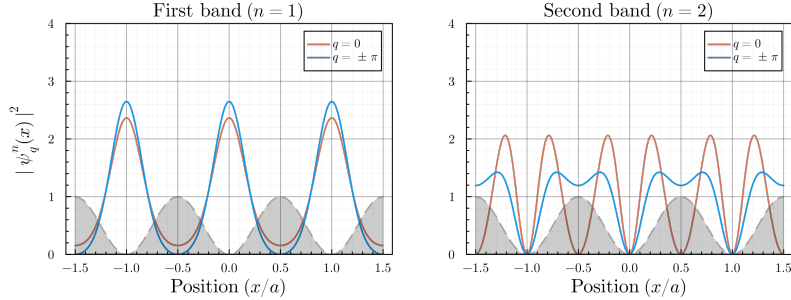


Figure 1.2: Probability distribution of Bloch wave-functions for $V_0 = 5E_r$. The lattice potential (black) is plotted to indicate the periodicity of the system.

1.2 Constructing a localized basis

While the bloch wavefunctions form a perfectly valid basis set for a periodic system, they are also delocalized across the entire lattice as seen in Fig. 2.2. Such a situation is rather cumbersome to work with, as will become clear in the next chapter when we discuss the formalism to describe many-particle physics. Instead, we look for a localized basis set.

A simple recipe can be obtained by drawing a parallel with the free-particle case once again. We know that the energy eigenstates are plane waves which are delocalized across all space, and performing a fourier transformation from $k \rightarrow x$ gives us dirac delta functions, which are highly localized. Similarly, the quasi-momentum q plays the role of k here and by performing a fourier transform over the first brillouin zone, we can construct a new basis by introducing a conjugate variable R that is analogous to x .

$$\phi_R^n(x) = \frac{1}{N} \sum_{q \in BZ} e^{-iqR} \psi_q^n(x) \quad (1.14)$$

where $\psi_q^n(x)$ are the bloch wave-functions of the n th band, N is the number of unit cells in the lattice and $\phi_R^n(x)$ are the so-called *Wannier* functions. An immediate consequence of the fourier transform is that these are no longer energy eigenstates, but that is a fair price to pay for a localized basis. Note that R extends over the lattice exactly in steps of the lattice spacing, a .

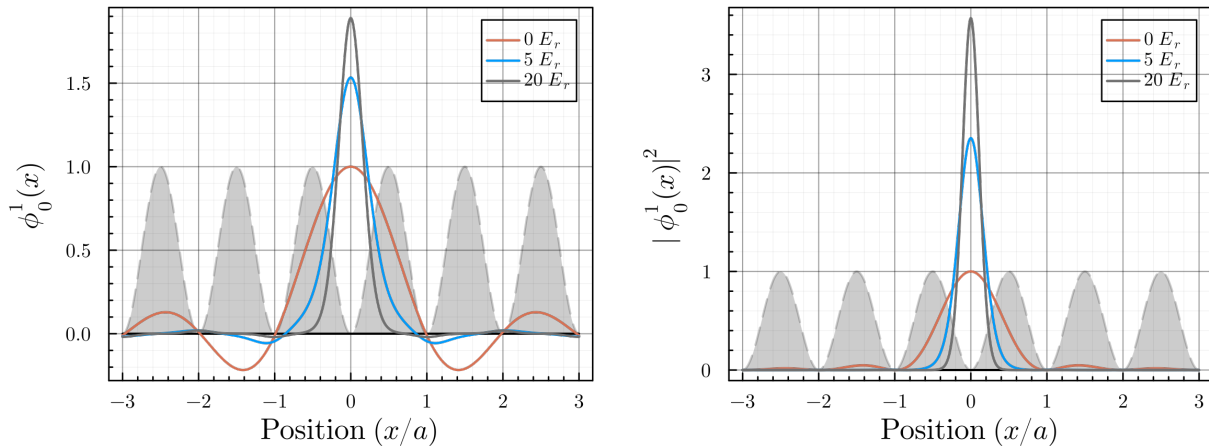


Figure 1.3: Probability amplitude and density of wannier wave-functions for wannier functions of the lowest band. The lattice potential (black) is plotted to indicate the periodicity of the system.

We see from Fig. 2.3 that as the lattice depth is increased, the wannier function becomes more localized. In fact, as mentioned earlier, a deep lattice potential can be approximated as a harmonic well and the corresponding Wannier function approaches a gaussian. Let

us now try to ascribe meaning to the conjugate index R that we have introduced, by considering the following expression for some $m \in \mathbb{Z}$.

$$\begin{aligned}\phi_{R+ma}^n(x) &= \frac{1}{N} \sum_{q \in BZ} e^{-iqR} e^{-iqma} \psi_q^n(x) \\ &= \frac{1}{N} \sum_{q \in BZ} e^{-iqR} \psi_q^n(x - ma) \\ &= \phi_R^n(x - ma)\end{aligned}$$

We see that translation in R corresponds to simply shifting the wannier function in real space by the same amount! This motivates the fact that R is simply an index to label the lattice site on which the wannier function is localized.

1.2.1 Gauge freedom and non-uniqueness

At this point, we also notice a peculiar feature of the Bloch wavefunctions, namely that there exists a gauge freedom in its definition.

$$\tilde{\psi}_q^n(x) \equiv e^{i\chi_n(q)} \psi_q^n(x) \quad (1.15)$$

where $\chi_n(q)$ can be any arbitrary function over the reciprocal lattice vectors and cannot be determined from the Schrodinger equation. More generally we can describe it in terms of a unitary operation, U , like so:

$$\tilde{\psi}_q^n(x) = \sum_{m=1}^N U_{mn}^{(q)} \psi_m^n(x) \quad (1.16)$$

$$\phi_R^n(x) = \frac{1}{N} \sum_{q \in BZ} e^{-iqR} \tilde{\psi}_q^n(x) \quad (1.17)$$

This gauge freedom clearly carries over to the Wannier functions, rendering them non-unique! Luckily, this does not change the fact that any choice of Wannier functions will still be localized, just that they may have different 'shapes'. This motivates the existence of a possibly unique set of Wannier functions that are *maximally localized*. For instance, such a set may be determined by minimizing the variance of the position operator.

$$\Omega = \sum_n \langle x^2 \rangle_n - \langle x \rangle_n^2 \quad (1.18)$$

Things can get even more complicated when the energy bands are close enough to intersect, in which case we must allow mixing of the wannier functions with respect to the n index as well. However, for the purpose of this thesis, we do not take these complexities into account and simply proceed with the choice of $\chi_n(q) = 0$. This suffices for a rough order of magnitude calculation to motivate the discussions in the following chapters.

CHAPTER

2

The Bose-Hubbard model

Now that we have set up the basic framework of single-particle physics in periodical potentials, we will proceed to use it to develop a description of the many-body system of bosons in an optical lattice.

2.1 Derivation

Consider a system of spinless bosons of mass m trapped in an optical lattice potential, $V_{\text{lat}}(r)$ with M sites. The physics of the system is described by the following second-quantized hamiltonian.

$$H = \int d^3r \cdot \Psi(r) \left[-\frac{\hbar^2}{2m} \nabla^2 + V_{\text{lat}}(r) \right] \Psi(r) + \frac{1}{2} \int d^3r \int d^3r' \Psi^\dagger(r) \Psi^\dagger(r') U_{\text{int}} \Psi(r) \Psi(r') \quad (2.1)$$

where $\Psi(r)$ and $\Psi^\dagger(r)$ are the bosonic field operators, fulfilling the bosonic commutation relations:

$$[\Psi(r), \Psi^\dagger(r')] = \delta(r - r') \quad [\Psi(r), \Psi(r')] = 0 \quad [\Psi^\dagger(r), \Psi^\dagger(r')] = 0 \quad (2.2)$$

Our first approximation can be motivated by noting the energy band gaps in Fig. 2.1. As long as the interaction energies of the trapped bosons are much smaller than the first energy gap, we can assume that the physics are mostly dominated by the lowest energy band. We can then expand the field operators in terms of a basis of wannier functions of the first band.

$$\Psi(r) = \sum_j \phi_j(r) \cdot a_j \quad (2.3)$$

where a_j (a_j^\dagger) creates (annihilates) a particle localized at the j -th lattice site in the lowest band. The bosonic operators a_j, a_j^\dagger satisfy the following commutation relations:

$$[a_j, a_l^\dagger] = \delta_{j,l} \quad [a_j, a_l] = 0 \quad [a_j^\dagger, a_l^\dagger] = 0 \quad (2.4)$$

Upon making this substitution, we arrive at the following hamiltonian:

$$H = - \sum_{i,j} t_{i,j} a_i^\dagger a_j + \frac{1}{2} \sum_{i,j,k,l} U_{i,j,k,l} a_i^\dagger a_j^\dagger a_l a_k \quad (2.5)$$

where $t_{i,j}$ and $V_{i,j,k,l}$ are defined as follows:

$$t_{i,j} = \int dx \cdot \phi_i(x) \left[-\frac{\hbar^2}{2m} \nabla^2 + V_{\text{lat}}(r) \right] \phi_j(x) \quad (2.6)$$

$$U_{i,j,k,l} = \frac{1}{2} \int \int dr_1 dr_2 \cdot \phi_i(r_1) \phi_j(r_2) U_{\text{int}}(r_1 - r_2) \phi_k(r_1) \phi_l(r_2) \quad (2.7)$$

For sufficiently deep optical lattices, only the nearest neighbour tunnelling amplitudes are significant ($t_{i,i+1} \gg t_{i,i+2}$) precisely because the wannier functions are highly localized. This motivates the tight-binding approximation where we neglect all the coupling terms beyond the nearest neighbors.

$$H = - \sum_{\langle i,j \rangle} t_{i,j} a_i^\dagger a_j + \frac{1}{2} \sum_{i,j,k,l} U_{i,j,k,l} a_i^\dagger a_j^\dagger a_l a_k \quad (2.8)$$

At this point, based on the type of interaction between the bosons, we can obtain various flavours of the model. For now, we will consider the simplest case of contact interaction, which is a pseudo-potential that we can introduce to model the low energy scattering physics.

$$U_{\text{int}}(r_1 - r_2) = \frac{4\pi\hbar^2 a_s}{m} \delta(r_1 - r_2) = g\delta(r_1 - r_2) \quad (2.9)$$

where a_s is the s-wave scattering length of the bosons. As a result of the short range nature of this interaction, there is only one non-zero matrix element from the interaction term, namely that of on-site repulsion, $U = U_{iiii}$. Upon considering an isotropic lattice ($t_{ij} \equiv t$, $U_{iiii} \equiv U$), we obtain the central theme of this thesis, the Bose Hubbard hamiltonian.

$$H = -t \sum_{\langle i,j \rangle} a_i^\dagger a_j + \frac{U}{2} \sum_i n_i(n_i - 1) \quad (2.10)$$

2.2 Ground state phases

To begin understanding the physics of this system, we note that it has two competing terms. The interplay between them gives rise to two distinct quantum phases that can be classified by analyzing the limiting cases of the hamiltonian. For simplicity, we will work in the grand-canonical ensemble with the hamiltonian, $H_{GCE} = H - \mu \sum_i n_i$.

2.2.1 Mott Insulator

Let us consider the limit $t \ll U$ of Eq. (3.10).

$$H = \frac{U}{2} \sum_i n_i(n_i - 1) - \mu \sum_i n_i \quad (2.11)$$

Such a hamiltonian only contains the pairwise on-site interaction energy of bosons occupying the same lattice site. We can think of $n_i(n_i - 1)/2$ as arising from nC_2 which counts the pairs of bosons on each site. This term tends to minimize the fluctuation of the occupation number by localizing the bosons onto the lattice sites.

Since Eq. (3.11) is simply a sum over single-site hamiltonians which are all equivalent, the ground state solution is a pure fock state.

$$|\Psi\rangle = \bigotimes_{i=1}^M |n\rangle = \underbrace{|n, n, \dots, n\rangle}_{M \text{ sites}} \quad (2.12)$$

with ground state energy $E_{gs} = \sum_i E_i$ such that:

$$E_i = \frac{U}{2}n(n-1) - \mu n \quad n = \left\lfloor \frac{\mu}{U} \right\rfloor + 1 \quad (2.13)$$

Thus, the Mott insulator phase is described by a state with integer occupation on each lattice site. Further, it is a gapped phase as it requires finite energy to generate excitations, and it is characterized by zero compressibility ($\partial N/\partial\mu = 0$).

2.2.2 Superfluid

Let us now consider the other limit, $t \gg U$ of Eq. (3.10).

$$H = -t \sum_{\langle i,j \rangle} a_i^\dagger a_j - \mu \sum_i n_i \quad (2.14)$$

This is simply a non-interacting tight-binding model in the second quantized notation. The 'hopping' term $a_i^\dagger a_j$ annihilates a particle at the j th site and creates a particle at the i th site. Such a hamiltonian tends to maximize the fluctuations of the occupation number by delocalizing the bosons across the entire lattice.

It is trivially diagonalizable by switching to the bloch basis ($\{\tilde{a}_k\}$):

$$a_i = \frac{1}{\sqrt{M}} \sum_k e^{-ikr_i} \tilde{a}_k \quad (2.15)$$

$$H = \sum_k (\epsilon_k - \mu) \tilde{a}_k^\dagger \tilde{a}_k \quad (2.16)$$

where ϵ_k is the dispersion relation determined based on the lattice geometry. The ground state is then simply a condensate in the $k = 0$ state:

$$|\Psi\rangle = (\tilde{a}_0^\dagger)^N |0\rangle = \left(\frac{1}{\sqrt{M}} \sum_{i=1}^M a_i \right)^N |0\rangle \quad (2.17)$$

For our purposes, we consider an interacting Bose-Einstein condensate to be equivalent to a superfluid. Although this is not strictly true, it is a reasonable assumption for our study. Such a phase can be described by a coherent state while working in the grand canonical ensemble. Further, it is also a gapless phase, as it requires arbitrarily small energy to generate excitations.

2.2.3 Quantum phase transition

From the above discussion, we see that the Mott insulator and Superfluid phases are quite distinct in their properties. Although this characterization was performed in the extreme limits, we expect that in the complete hamiltonian, Eq. (3.10), the true phases would broadly have the same properties. The true ground states, however, may be different due to the presence of particle-hole excitations.

As a result, even at $T = 0$, we expect a transition to occur between the Mott insulator and Superfluid phases. Such a transition is facilitated by quantum fluctuations rather than thermal ones. In the next chapter, we will try to generate the corresponding phase diagram using various numerical techniques.

2.3 Connecting theory and experiment

Before we proceed further, it is prudent to note that the Bose Hubbard parameters, t and U are not independent as is apparent from the derivation in Sec. 3.1. We will explore this fact by explicitly computing these parameters for a 1D lattice.

Let us begin with the hopping parameter as defined in Eq. (3.6) and perform some manipulations to recast it into a surprisingly succinct form.

$$\begin{aligned}
t_{ij} &= - \int d^3r \phi_i^* \left[-\frac{\hbar^2}{2m} \nabla^2 + V_{\text{lat}}(r) \right] \phi_j \\
&= - \int d^3r \left(\frac{1}{\sqrt{N}} \sum_q e^{iq \cdot r_i} \psi_q^* \right) \left[-\frac{\hbar^2}{2m} \nabla^2 + V_{\text{lat}}(r) \right] \left(\frac{1}{\sqrt{N}} \sum_{q'} e^{iq' \cdot r_i} \psi_{q'} \right) \\
&= - \frac{1}{N} \sum_{qq'} e^{iq \cdot r_i} \cdot e^{iq' \cdot r_i} \int d^3r \psi_q^* \left[-\frac{\hbar^2}{2m} \nabla^2 + V_{\text{lat}}(r) \right] \psi_{q'} \\
&= - \frac{1}{N} \sum_{qq'} e^{iq \cdot r_i} \cdot e^{iq' \cdot r_i} \cdot \delta_{qq'} \epsilon_q \\
t_{ij} &= - \frac{1}{N} \sum_q \epsilon_q \cdot e^{iq \cdot (r_i - r_j)} \tag{2.18}
\end{aligned}$$

where ϵ_q is the dispersion relation. This tells us that the tunneling amplitude is simply a Fourier transform of the energy dispersion of the system. On the other hand, the on-site

interaction parameter is computed quite directly from Eq. (3.7) as follows.

$$U = g \int d^3r |w(r)|^4 \quad (2.19)$$

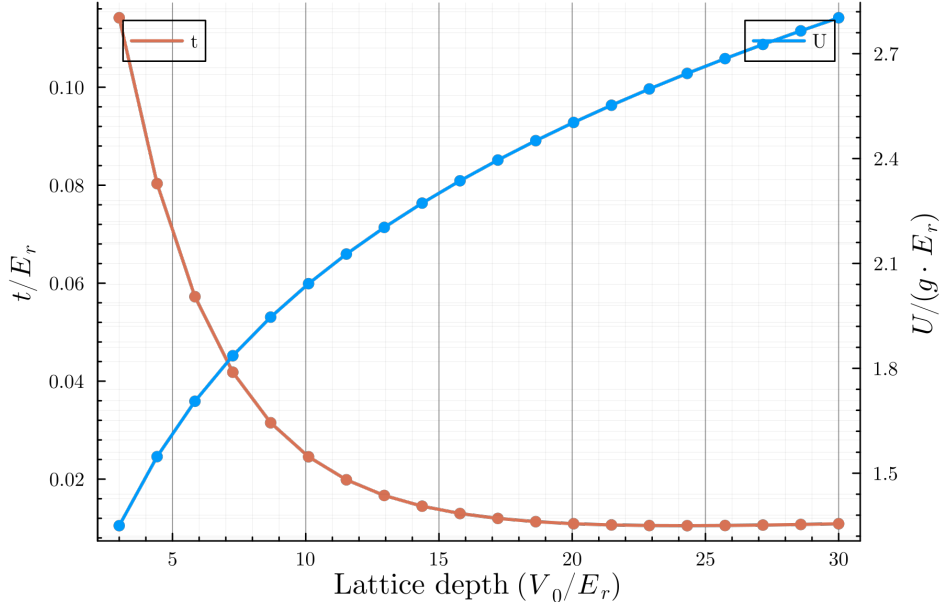


Figure 2.1: Bose Hubbard parameters in a 1D system for various lattice depths.

We see that the parameters are quite dependant in Fig. 3.1. At this point, it seems that once we have fixed the lattice potential (and hence, the wannier functions upto a gauge), the parameters t and U are uniquely determined. This would severely restrict the regimes of the Bose-Hubbard model that are experimentally accessible. However, we have not taken into the account the co-efficient g in the interaction parameter. Particularly, the s-wave scattering length a_s can be tuned using Feshbach resonances, thus restoring our ability to explore the parameter space.

For the rest of this thesis, we will study the phase diagram of the Bose-Hubbard model as if t and U are independant, in order to gain a complete understanding of the various phases hosted by it. However, experimentally traversing these diagrams would require the construction of paths by taking their dependance into account.

CHAPTER

3

Solving the Bose-Hubbard model

Consider the 1D Bose-Hubbard hamiltonian, with N bosons and M lattice sites:

$$H = -t \sum_{\langle i,j \rangle} a_i^\dagger a_j + \frac{U}{2} \sum_i n_i(n_i - 1) - \mu \sum_i n_i \quad (3.1)$$

In this chapter, we will review some numerical techniques to study the phases exhibited in this model. Although the 1D model is exactly solvable using a Bethe ansatz, these techniques are easily extended to higher dimensions and other lattice geometries where an exact solution is not known.

3.1 Exact Diagonalization

We begin with the most naive approach of exactly diagonalizing the hamiltonian. A natural basis to construct the many-body hamiltonian is the set of fock states, $\{|n_1, n_2, \dots, n_M\rangle\}$ defined as the simultaneous eigenstates of the site-wise number operators.

$$\hat{n}_i |n_1, n_2, \dots, n_M\rangle = n_i |n_1, n_2, \dots, n_M\rangle \quad (3.2)$$

such that $\sum_{i=1}^M n_i = N$ and $n_i \geq 0$.

Constructing this basis is equivalent to combinatorics problem of enumerating all the ways of distributing N objects in M boxes. It follows that the dimensionality of the Hilbert space is given by, $d = (M + N - 1)! / N!(M - 1)!$. We can now compute the matrix elements of the hamiltonian, $\langle u | H | v \rangle$, using the following relations that can be obtained directly from the bosonic commutation relations in Eq. (3.4).

$$\hat{a}_i |n_1, n_2, \dots, n_i, \dots, n_M\rangle = \sqrt{n_i} |n_1, n_2, \dots, n_i - 1, \dots, n_M\rangle \quad (3.3)$$

$$\hat{a}_i^\dagger |n_1, n_2, \dots, n_i, \dots, n_M\rangle = \sqrt{n_i + 1} |n_1, n_2, \dots, n_i + 1, \dots, n_M\rangle \quad (3.4)$$

Due to the large dimension of such a matrix, a complete diagonalization would be computationally expensive and wasteful since we only aim to study the ground state properties. As a result, an iterative procedure such as the Lanczos algorithm would be a better choice since it only computes the extreme eigenvalues and eigenvectors of large matrices. We now proceed to discuss some observables that can be used to track the phase transition.

Single Particle Density Matrix

Consider the quantity $n^{(1)}(r, r') = \langle \Psi(r)^\dagger \Psi(r') \rangle$ where $\Psi(r), \Psi(r')$ are the bosonic field operators introduced in Eq. (3.1). This is a matrix with respect to (r, r') and can be used to formulate a rigorous definition of a BEC by writing it in its diagonal form.

$$\begin{aligned} n^{(1)}(r, r') &= \sum_i n_i \cdot \psi^*(r) \psi(r') \\ &= n_0 \cdot \phi_0(r)^* \phi_0(r') + \sum_{i \neq 0} n_i \cdot \psi^*(r) \psi(r') \end{aligned} \quad (3.5)$$

where n_i and $\{\psi_i(r)\}$ are the eigenvalues and single-particle eigenstates of $n^{(1)}(r, r')$, respectively. These states $\{\psi_i(r)\}$ are not necessarily eigenstates of the single-particle hamiltonian.

Note that we have separated the term with the largest eigenvalue (n_0) from the sum. We can now define a condensate fraction, $f = n_0/N$, which will be macroscopic ($f \sim 1$) when the system is in a BEC phase and vanishes otherwise. As a result, when we consider the limit $|r - r'| \rightarrow \infty$ in the BEC phase, while most of the sum will interfere destructively and cancel out, the first term may have a non-zero contribution.

$$\lim_{|r - r'| \rightarrow \infty} n^{(1)}(r, r') \neq 0 \quad (3.6)$$

This condition is known as Off-Diagonal Long-Range Order (ODLRO), and will be useful in deriving the order parameter in the mean-field analysis.

3.1.1 Results

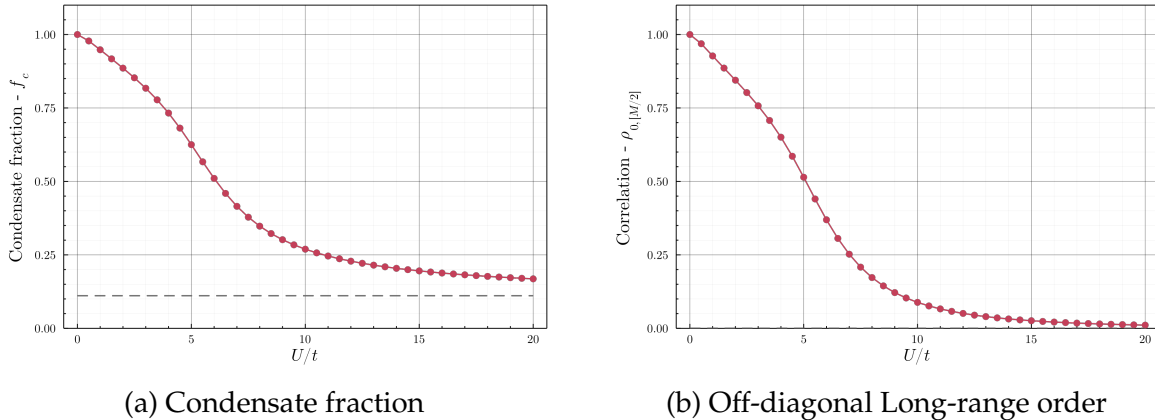


Figure 3.1: Tracking the phase transition using various observables ($N = M = 9$)

We see in Fig. 4.1a that the condensate fraction, f , quickly drops from 1 as U/t is increased. However, note that it never vanishes even for arbitrarily small U/t , against our expectations

for the Mott insulator phase. This turns out to be an artifact of the finite size of the system. Since the eigenvalues of the SPDM must satisfy $n_0 \geq 1$, we have $f \geq 1/M$ which would vanish for large M .

On the other hand, in Fig. 4.1b we have plotted the matrix element of the SPDM with the farthest indices, in an attempt to capture the ODLRO condition. Surprisingly, we do see that the element starts off at 1 and quickly vanishes in the Mott insulator regime, even though the condition of $|i - j| \rightarrow \infty$ cannot really be achieved in such a small system.

There is also another observable that is worth tracking, namely, the average variance of the number operator on an arbitrary lattice site, $\langle \delta n^2 \rangle$. Since the Mott insulator phase is expected to be a pure fock state, the occupation variance must vanish.

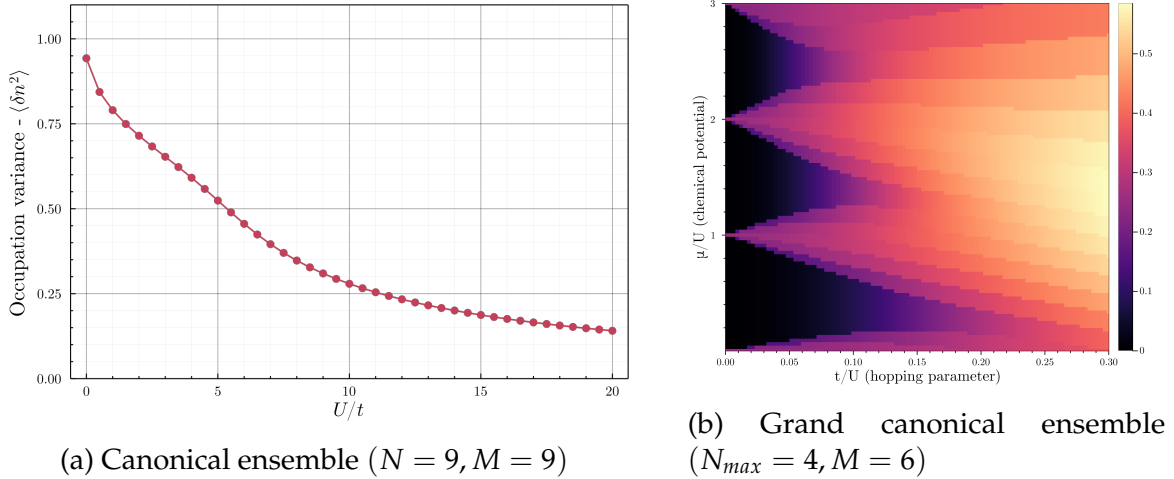


Figure 3.2: Tracking the phase transition using average variance of occupation number

Unsurprisingly, Fig. 4.2a, also demonstrates a curve with a similar trend as the ones in Fig. 4.1. Although there seems to be some signatures of the quantum phase transition, it seems that the Mott insulator phase strictly only exists for $U/t \rightarrow \infty$ ($\implies t/U = 0$). However, note that these results were obtained from an exact diagonalization over a fixed- N subspace of the fock space. If we allow variable particle number (upto an arbitrary cut-off, $N \in [0, N_{max}]$) by considering a grand canonical ensemble instead, we can gain some further insight. We see that this is indeed the case, as the phase diagram obtained in Fig. 4.2b suggests that the Mott insulator phase could exist in an extended region away from $t/U = 0$.

However, it is dubious to make this claim rigorously since all of our possible order parameters are muddled by the finite (and small!) lattice size that we have considered. One could perform this analysis by exactly diagonalizing a larger system, however, the computational cost increases exponentially and quickly becomes unfeasible after ~ 20 sites. As a result, we will proceed to explore some approximate methods that allow us to get more qualitative

but well-defined results.

3.2 Mean Field Theory

The motivation for this technique is the fact that diagonalizing the BHM in either of the extreme limits is trivial, however the Hilbert space blows up in the general case, Eq. (4.1). Note that we will continue working exclusively in the grand canonical ensemble.

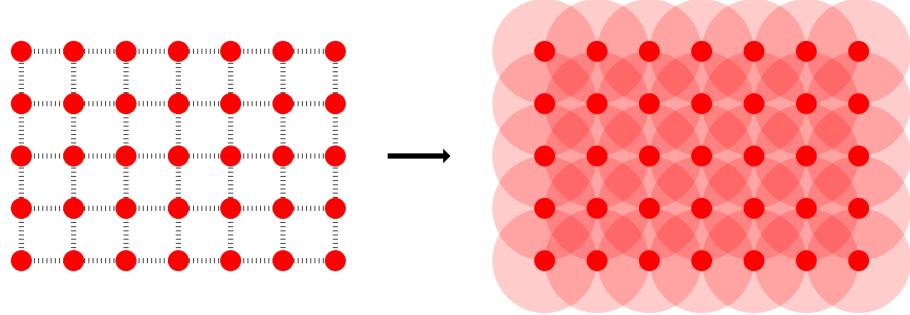


Figure 3.3: Pictorial representation of MFT in 2D

In order to extract some qualitative features of the model, we attempt a de-coupling which results in a system with a smaller Hilbert space. To facilitate this, we will replace the site operators with their expectation values and ignore the higher order fluctuations.

$$\begin{aligned} \hat{a}_i &= \Psi_i + \delta\hat{a}_i \\ \implies \delta a_i^\dagger \delta a_j &= (a_i^\dagger - \Psi_i^*)(a_j - \Psi_j) \approx 0 \\ \implies a_i^\dagger a_j &\approx \Psi_j a_i^\dagger + \Psi_i^* a_j - \Psi_i^* \Psi_j \end{aligned} \quad (3.7)$$

We can now de-couple the hopping term like so:

$$\begin{aligned} -H_{hop}/t &= \sum_{\langle i,j \rangle} a_i^\dagger a_j \\ &= \sum_{\langle i,j \rangle} (\Psi_j a_i^\dagger + \Psi_i^* a_j - \Psi_i^* \Psi_j) \\ &= \sum_i \left(\sum_{j \in N_i} \Psi_j \right) a_i^\dagger + \sum_i \left(\sum_{j \in N_i} \Psi_j^* \right) a_i - \sum_i \left(\sum_{j \in N_i} \Psi_j \right) \Psi_i^* \end{aligned} \quad (3.8)$$

where N_i is the set of nearest neighbour indices for the lattice site i . Defining the mean order parameter, $\bar{\Psi}_i = \frac{1}{z} \sum_{j \in N_i} \Psi_j$, where z is the coordination number of the lattice, we obtain:

$$-H_{hop}/zt = \sum_i (\bar{\Psi}_i a_i^\dagger + \bar{\Psi}_i^* a_i - \bar{\Psi}_i \bar{\Psi}_i^*) \quad (3.9)$$

We can then write the entire site-decoupled hamiltonian which depends on a set of M mean-field parameters, $\{\Psi_i\}$ as follows.

$$H_{MF}\{\Psi_i\} = \sum_i H_i\{\Psi_i\} \quad (3.10)$$

$$H_i\{\Psi_i\} = -zt(\bar{\Psi}_i a_i^\dagger + \bar{\Psi}_i^* a_i - \bar{\Psi}_i \bar{\Psi}_i^*) + \frac{U}{2} n_i(n_i - 1) - \mu n_i \quad (3.11)$$

The complexity of the problem is drastically reduced now that we only have to solve M single-site hamiltonians. Such a mean-field decoupling effectively proposes the following product ansatz for the wavefunction:

$$|\Psi\rangle = \bigotimes_{i=1}^M \left(\sum_{n=0}^{\infty} f_{i,n} |n\rangle \right) \quad (3.12)$$

This is in-fact equivalent to the Gutzwiller Mean-field approach, wherein the co-efficients $f_{i,n}$ are obtained such that the ground state energy is minimized. We will however utilize a self-consistent scheme to obtain the ground state solution.

Due to the translational symmetry of the system, we can further simplify the hamiltonian by setting $\Psi_i = \Psi$. It then follows that $\bar{\Psi} = \Psi$. Further, due to the $U(1)$ symmetry (invariance under a global phase shift, $\hat{a}_i \rightarrow e^{i\theta} \hat{a}_i$) of the BHM, we can assume that $\Psi \in \mathbb{R}$ without loss of generality.

$$H_i\{\Psi\} = -zt\Psi(a_i + a_i^\dagger) + \frac{U}{2} n_i(n_i - 1) - \mu n_i + zt|\Psi|^2 \quad (3.13)$$

3.2.1 Numerical solution

Since all the single-site hamiltonians are equivalent, it is sufficient to solve any one of them and we will drop the index i henceforth. It might then seem that we can trivially diagonalize $H\{\Psi\}$ to study the system. However, there are still a few considerations to be made.

Firstly, in order to construct the matrix form of $H\{\Psi\}$, the local number basis ($\{|n\rangle\}|_{n=0}^{\infty}$) seems to be an obvious choice. However, this would give rise to an infinite dimensional matrix, so we must choose to truncate the basis at some n_{max} . We will discuss this further in Sec. 4.2.4.

Secondly, $H\{\Psi\}$ is parametrized by the mean-field parameter, Ψ , which is required to construct the matrix. But by definition, we have $\Psi = \langle \psi_{gs} | \hat{a} | \psi_{gs} \rangle$ which can only be computed by diagonalizing the hamiltonian. Thus, the parameter Ψ must be determined in a self-consistent manner. This can be described in a formal way by wrapping this procedure into a function.

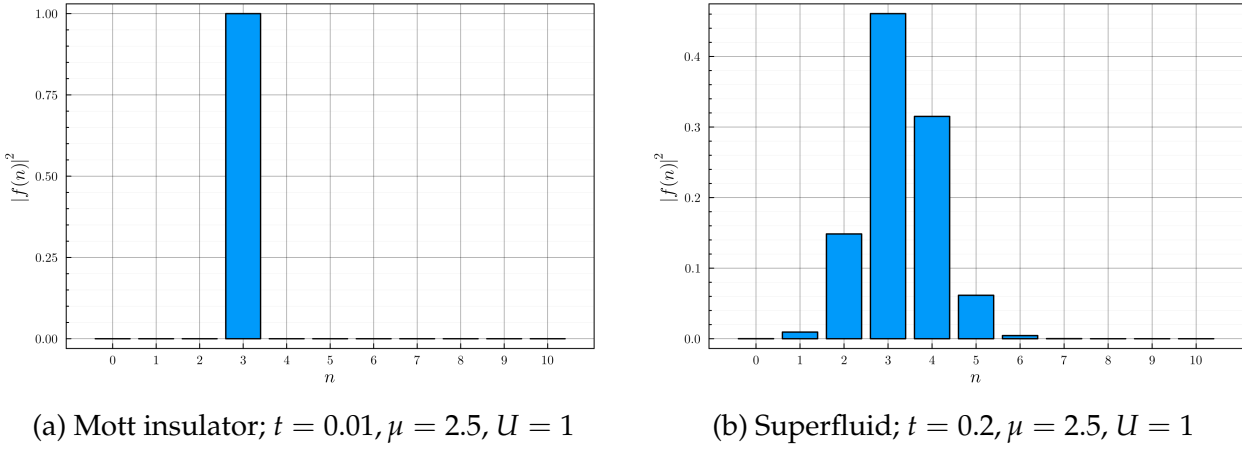
$$f(\Psi) \rightarrow \text{Diagonalize } H\{\Psi\} \text{ and compute } \psi_{gs} \rightarrow \langle \psi_{gs} | \hat{a} | \psi_{gs} \rangle \quad (3.14)$$

Solving the self-consistency loop is equivalent to finding the fixed point Ψ^* such that $f(\Psi^*) = \Psi^*$. One can now utilize the machinery of non-linear dynamics and root-finding techniques to solve this problem.

The most direct (and ubiquitous) method to proceed with is Fixed Point Iteration. This involves starting with an initial guess $\Psi^{(0)}$, and computing $\Psi^{(n)} = f(\Psi^{(n-1)})$ repeatedly until it converges within a specified tolerance. Such a method can be highly sensitive to the choice of initial guess, and there is no guarantee of convergence nor a bound on how fast it happens. However, these issues can be ignored for now and do not crop up until much further in the thesis.

3.2.2 Plotting the phase diagram

Before we proceed, it is important to note that the mean-field hamiltonian clearly changes certain features of the original hamiltonian. A striking example of this is that while Eq. 4.1 conserves the particle number, Eq. 4.11 does not! It seems then that our 'choice' of working in the grand canonical ensemble is strictly necessary at the mean-field level. At this point, we must ask whether such a hamiltonian can still admit phases that can be classified as a Mott insulator or a superfluid.



(a) Mott insulator; $t = 0.01, \mu = 2.5, U = 1$

(b) Superfluid; $t = 0.2, \mu = 2.5, U = 1$

Figure 3.4: Distribution of co-efficients in fock basis

Solving the mean-field hamiltonian for various parameter choices results in two distinct phases as seen in Fig. 4.4. The Mott insulator phase is captured as a pure fock state with fixed occupation number on each lattice site. On the other hand, the superfluid phase is captured as a coherent state, which is a well-known means of describing BECs. This can be understood as the ground state picking up a random phase, $e^{i\theta}$, due to spontaneous breaking of the $U(1)$ symmetry. Further, the idea of particle number conservation can be loosely recovered by considering the thermodynamic limit wherein $\sqrt{\langle \delta n^2 \rangle} / \langle n \rangle \rightarrow 0$ as $N, M \rightarrow \infty$. In case this explanation is unsatisfactory, there is a way to formulate this

scheme without ever breaking the number conservation, but the analysis becomes far more cumbersome.

Now that we have confirmed that ground state can admit these phases, we require an order parameter to distinguish them. A simple quantity presents itself by considering the definition of off-diagonal long-range order from Eq. (4.6) as a means of identifying BECs.

$$\lim_{|i-j| \rightarrow \infty} \langle a_i^\dagger a_j \rangle = \lim_{|i-j| \rightarrow \infty} \langle a_i^\dagger \rangle \langle a_j \rangle = \Psi_i^* \Psi_j = |\Psi|^2 \neq 0 \quad (3.15)$$

Note that such a decoupling is only valid at the mean-field level. We can clearly see now that the idea of spontaneous $U(1)$ symmetry breaking is captured by this result. Thus, we can use the mean-field parameter Ψ as the superfluid order parameter as well.

We can now naively plot the phase diagram by computing the ground-state solution and hence the order parameter over a grid of μ/U and t/U values.

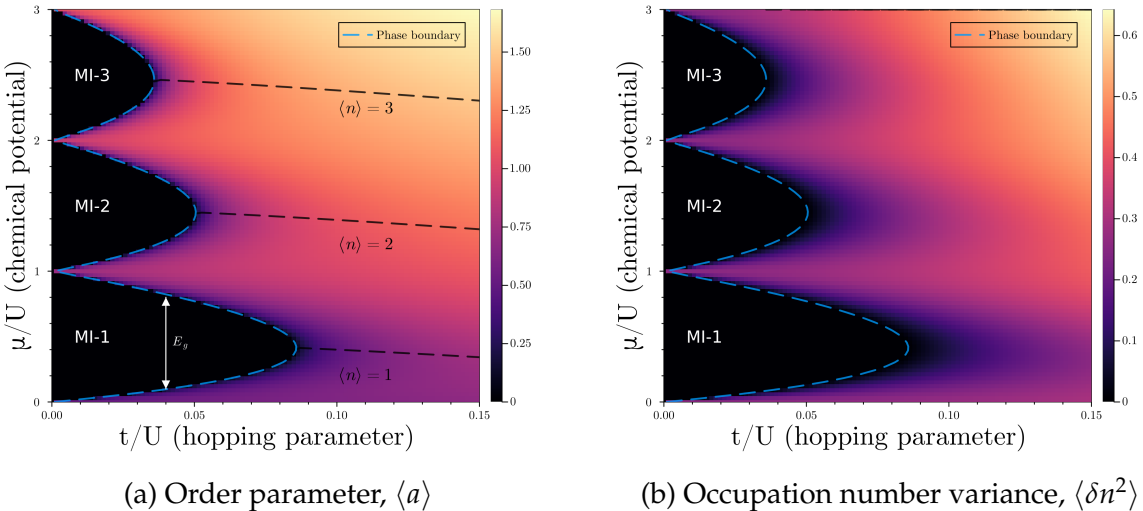
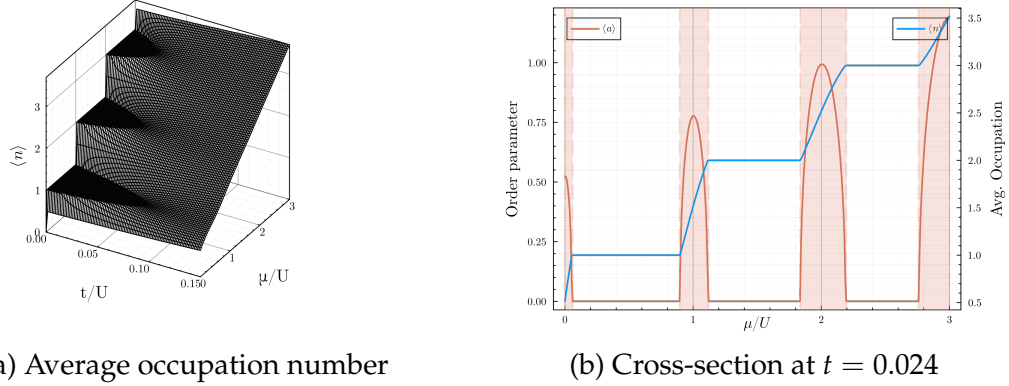


Figure 3.5: 1D Mean-field phase diagram

A clean phase diagram is obtained in Fig 4.5a, where the Mott insulator phase manifests as lobes in the $t - \mu$ plane. We also note from Fig. 4.5b that the occupation number variance serves as an equally valid order parameter, giving us the same phase diagram. We can get further insight into the nature of the Mott lobes by plotting the average occupation number as well.



(a) Average occupation number

(b) Cross-section at $t = 0.024$

Figure 3.6: Distinguishing phases using the average occupation

As expected, Fig. 4.6 shows the existence of integer occupation plateaus corresponding to the points where the order parameter vanishes in the phase diagram. As the chemical potential is increased, there is a sudden jump to the next Mott lobe admitting one more boson per lattice site. Further, for a given point inside a Mott lobe, the vertical distance to the lower (upper) arm denotes the energy required to excite a hole (particle), thus implying that the Mott insulator is indeed a gapped phase.

We also note that the MI-SF transition is second order since the order parameter changes continuously across the boundary. As a result, one can also perturbatively treat the hopping term in Eq. 4.11 to directly obtain an analytic expression for the phase boundary. This matches exactly with our numerical results since the perturbative term is proportional to Ψ , which can be chosen to be arbitrarily small near the phase boundary.

3.2.3 A better technique

Although the grid-based approach gives us a qualitative idea of the phase diagram, the accuracy of the phase boundary is limited by the discretization of the grid. However, the fact that there is only a single transition along t for a fixed value of μ lets us utilize a bisection method to determine the transition point, t_c . Performing this for a grid of values of μ gives us the phase boundary such that the error falls as $1/2^n$ for n bisections.

But we can do even better! To utilize the bisection method, at any given point we only require the information of the ground state phase, i.e, the rest of the information contained in the ground-state is unnecessary. A naive approach would be to directly check if $\Psi = 0$ is a fixed point of the self-consistency function in Eq. 4.14. However, it turns out that $\Psi = 0$ is *always* a fixed point, but is unstable for the superfluid phase. In order to find another approach, let us analyze the nature of convergence of the self-consistent procedure.

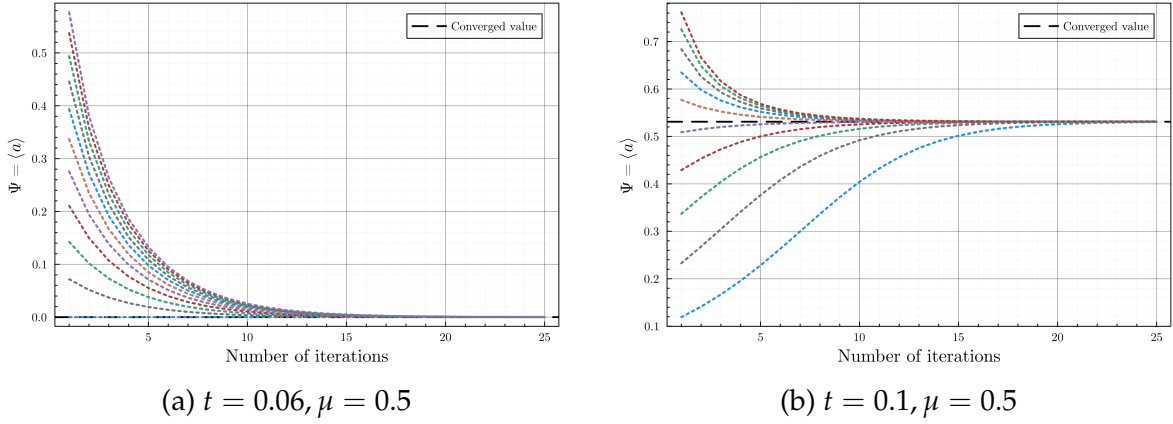


Figure 3.7: Monotonic convergence of self-consistency loop

It is apparent from Fig. 4.7 that fixed-point iteration always monotonically converges to the stable fixed point. This means that using a small initial guess such as $\Psi^{(0)} = 1e-9$, we can determine whether $\Psi = 0$ is a stable fixed point with a single iteration!

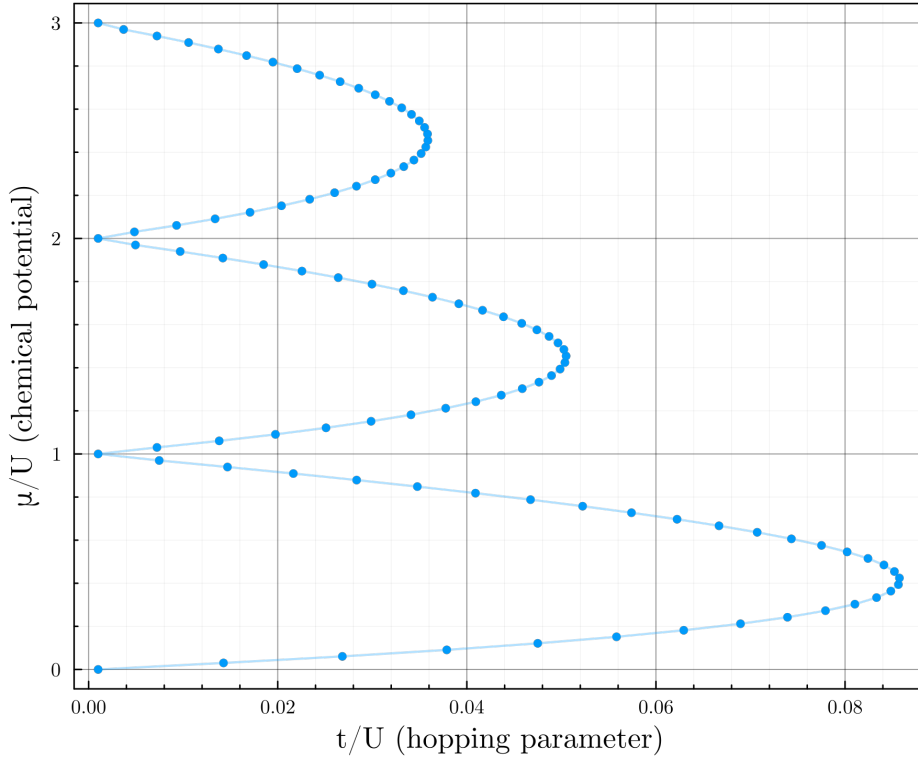


Figure 3.8: 1D Mean-field phase boundary determined by the bisection technique

3.2.4 Determining n_{max}

Before wrapping up, we must tackle the issue of dealing with an infinite dimensional hamiltonian. Truncating the hilbert space at an arbitrary occupation number might seem like it fundamentally changes the model under consideration. The extreme limit of this is setting $n_{max} = 1$ corresponding to a system of hard-core bosons, and any higher truncation amounts to considering semi-hardcore bosons of sorts.

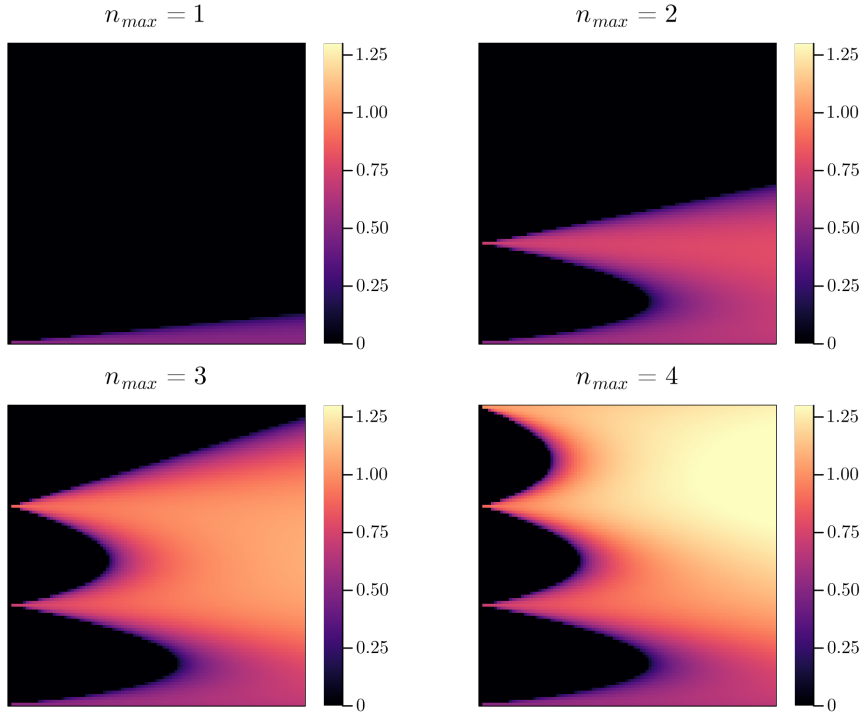


Figure 3.9: Qualitative variation of phase diagram as the occupation cutoff is increased.

Most notably, there will only be n_{max} Mott lobes and for larger chemical potential, the entire parameter space will remain a mott insulator since the maximum number of bosons is capped. However, it turns out that this is a minor issue upon realizing that the physics of the low-energy lobes remain largely unaffected upon truncation and discrepancies only arise closer to the higher order lobes. This is demonstrated in Fig. 4.9 and can be checked rigorously by computing the convergence of the phase boundaries as n_{max} is increased.

In this thesis, we mostly focus on the first three Mott lobes, and the corresponding phase boundaries are found to converge quickly as n_{max} is increased upto a value of 10.

3.2.5 Extending to finite temperature

In this section, we see that the mean-field approach is capable of handling finite temperature calculations as well. The only change required is to compute the expectation values as

thermal expectations, by taking into account all the states with boltzmann weights. The self-consistency relation $\Psi = \langle a \rangle_T$ can be recovered as well by imposing minimization of the free energy.

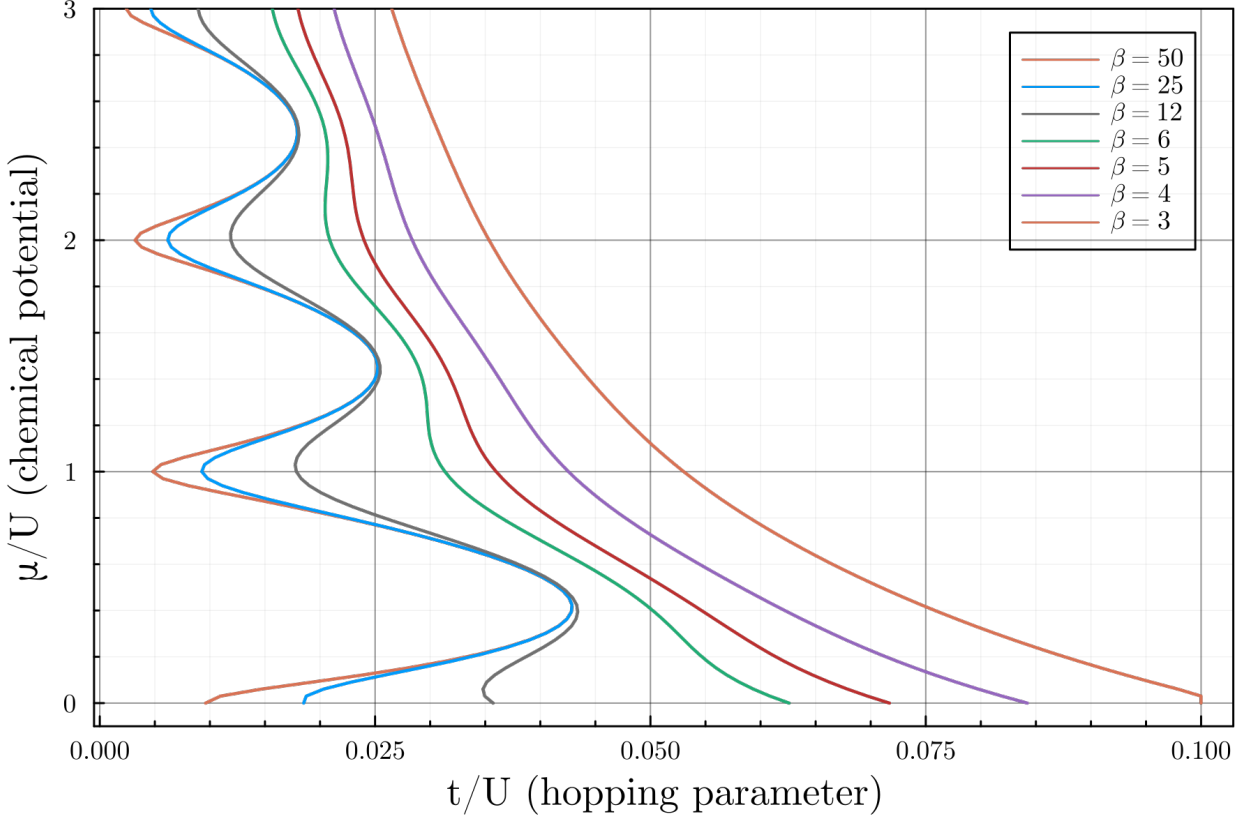


Figure 3.10: 1D Mean-field phase boundaries at finite temperatures.

At a finite temperature, Fig. 4.10 seemingly shows that the Mott insulator lobes coalesce into a single region as the temperature is increased. However, this is infact due to the existence of a thermally disordered phase, namely, the normal fluid. At the mean field level, it is remarkably similar to the Mott insulator except that it has a finite compressibility. In fact, at any $T \neq 0$, the compressibility gains a non-zero value for all parameters, implying that a Mott insulator ceases to exist at finite temperature. In general though, an arbitrary cut-off can be chosen for the compressibility to distinguish the normal fluid and Mott insulator phases.

3.2.6 An alternative de-coupling

Decoupling the hopping term ($a_i^\dagger a_j$) seems ubiquitous in literature when trying to simplify the Bose-Hubbard model. Strangely, the standard scheme for the mean-field study of the (fermionic) Hubbard model involves decoupling the interaction term instead. Nothing

stops us apriori from utilizing a similar scheme as well.

$$\begin{aligned}\hat{n}_i &= \rho_i + \delta\hat{n}_i \\ \implies \delta n_i^2 &= (n_i - \rho_i)(n_i - \rho_i) \approx 0 \\ \implies n_i^2 &\approx 2\rho_i n_i - \rho_i^2\end{aligned}\tag{3.16}$$

The hamiltonian can then be written as:

$$H_{MF} = -t \sum_{\langle i,j \rangle} a_i^\dagger a_j + \sum_i \left(\mu - \frac{U}{2} + U\rho_i \right) n_i - \frac{U}{2} \sum_i \rho_i^2\tag{3.17}$$

If we utilize translational symmetry to set $\rho_i = \rho$ and switch to the bloch basis, we get:

$$H_{MF} = -t \sum_k \left(\epsilon_k + \mu - \frac{U}{2} + U\rho \right) \tilde{a}_k^\dagger \tilde{a}_k - \frac{U}{2} M \rho^2\tag{3.18}$$

Since this is already diagonal, the ground state would simply be a condensate in the k -mode with lowest energy. Note that such a decoupling still preserves the conservation of particle number and as a result, $\langle a \rangle$ can no longer serve as an order parameter for the superfluid phase. Regardless, we see that a Mott insulator can never be admitted as a ground state by such a hamiltonian since it is always a condensate. This exercise brings to light an apparent subjectivity involved in choosing an appropriate decoupling. However, although the choice may be guided by considering the limiting behaviour of the system, the right choice is the one that generates the lowest ground state energy. Such a claim can be made rigorous if we view the mean field treatment as a variational method.

3.2.7 Pitfalls

Although the mean-field approach has allowed us to gain some insight on the BHM, it is only reliable for qualitative results. Particularly, since we have ignored higher order quantum fluctuations, we tend to over-estimate the extent of the ordered phase. Further, most of the information about the lattice geometry and dimensionality is lost as we only take into account the co-ordination number of each lattice site. We will now proceed to formulate a numerical technique that tackles these issues.

3.3 Cluster Mean Field Theory

This technique can be seen a middle ground between exact diagonalization and single-site mean field theory as portrayed in Fig. 4.11.

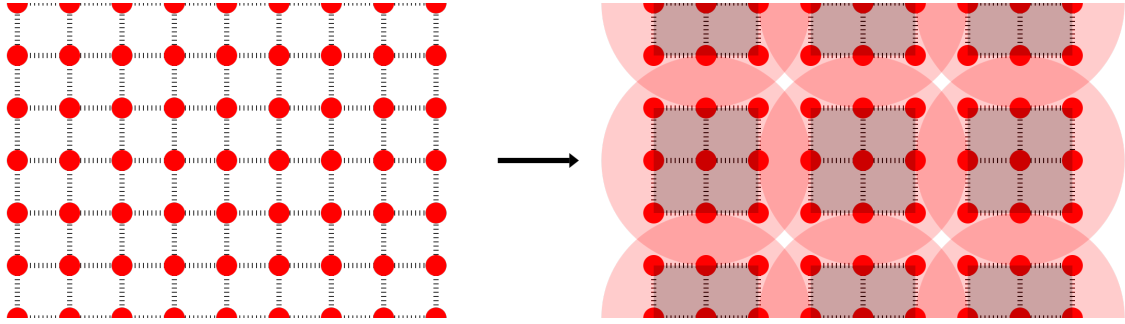


Figure 3.11: Pictorial representation of CMFT in 2D

We demonstrate the idea by considering a 1D lattice with M sites. The chain can then be divided into N_c clusters, each of length L such that $M = LN_c$. The hopping term of the BHM can now be written as follows.

$$H_{hop} = -t \sum_{j=0}^{N_c-1} \sum_{l=1}^{L-1} (a_{Lj+l}^\dagger a_{Lj+l+1} + a_{Lj+l+1}^\dagger a_{Lj+l}) - t \sum_{j=0}^{N_c-1} (a_{Lj+L}^\dagger a_{Lj+L+1} + a_{Lj+L+1}^\dagger a_{Lj+L}) \quad (3.19)$$

where the first term, H_{intra} couples the sites within each cluster, and the second term, H_{inter} couples the different clusters. The main idea of CMFT is to treat the intra-cluster coupling exactly and the inter-cluster coupling at a mean-field level. Following the same de-coupling we used in Eq. (4.7), we obtain:

$$H_{\text{intra}} = -t \sum_{j=0}^{N_c-1} [(a_{Lj+L}^\dagger + a_{Lj+L+1}^\dagger) \Psi + (a_{Lj+L} + a_{Lj+L+1}) \Psi^*] + 2tN_c |\Psi|^2 \quad (3.20)$$

where $\Psi = \langle a_i \rangle$ is the mean-field order parameter. Putting all this together, we arrive at the cluster-decoupled hamiltonian.

$$H_{MF}\{\Psi\} = \sum_{j=0}^{N_c-1} H_{MF}^L\{\Psi\} = \sum_{j=0}^{N_c-1} (H_j^L + V_j^L\{\Psi\}) \quad (3.21)$$

$$H_j^L = -t \sum_{l=1}^{L-1} (a_{Lj+l}^\dagger a_{Lj+l+1} + a_{Lj+l+1}^\dagger a_{Lj+l}) + \frac{U}{2} \sum_{l=1}^L n_{Lj+l} (n_{Lj+l} - 1) - \mu \sum_{l=1}^L n_{Lj+l} \quad (3.22)$$

$$V_j^L\{\Psi\} = -t(\Psi(a_{Lj+1}^\dagger + a_{Lj+L}^\dagger) + \Psi^*(a_{Lj+1} + a_{Lj+L})) + 2t|\Psi|^2 \quad (3.23)$$

Again, without loss of generality one can assume $\Psi \in \mathbb{R}$ and solve the system in a self-consistent manner. This procedure largely remains the same for other lattice geometries but requires more book-keeping as we are forced to include more mean-field parameters (one for each distinct kind of boundary site in the cluster).

3.3.1 Results

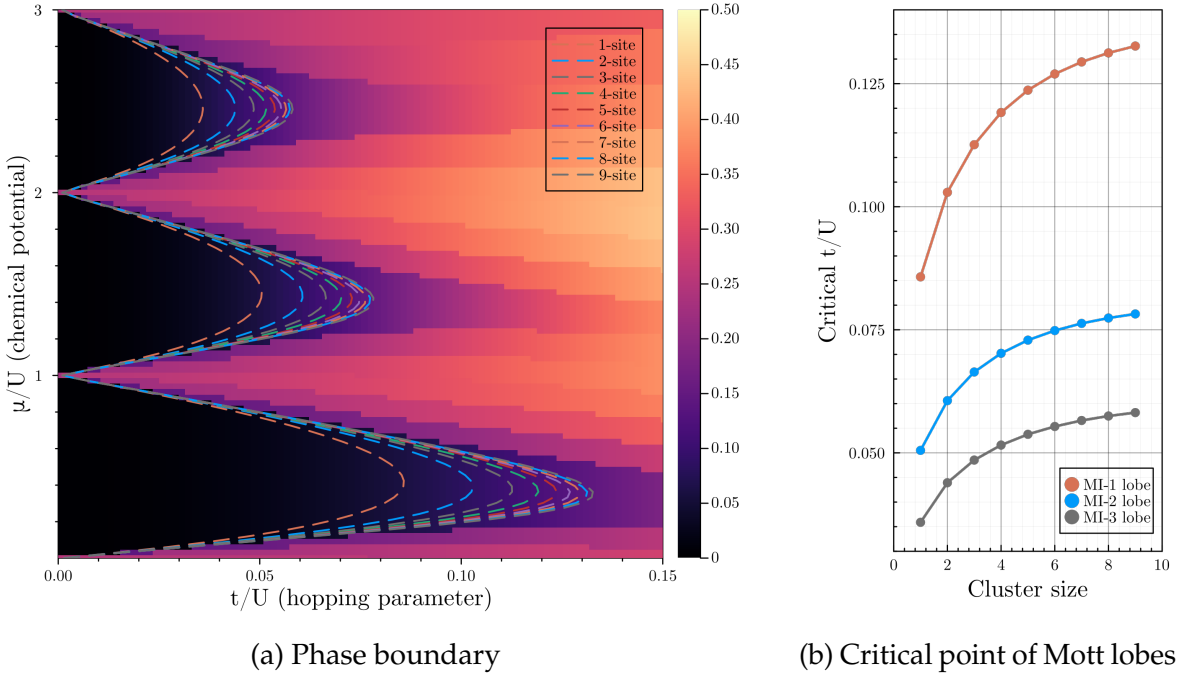


Figure 3.12: Comparison of 1D CMFT results for various cluster sizes

We see that the estimation of the phase boundaries improves as we increase the size of the cluster. However, while the computational cost still grows exponentially, the marginal improvement of the boundary diminishes for larger cluster sizes. Although this might only be the case for 1D systems, we decide not to employ this technique for further analysis due to the complexity involved in an implementation for arbitrary lattice geometries.

CHAPTER

4

Dipolar bosons in a lattice

In this chapter, we consider spinless bosons that have a permanent dipole moment and are trapped in a lattice. Since dipole-dipole interactions fall off as $V(r) \sim 1/r^3$, the contact interaction alone results in a poor description of the system. To remedy this, we take into account the nearest neighbour interactions as well.

$$H = -t \sum_{\langle i,j \rangle} a_i^\dagger a_j + \frac{U}{2} \sum_i n_i(n_i - 1) + \frac{V}{2} \sum_{\langle i,j \rangle} n_i n_j - \mu \sum_i n_i \quad (4.1)$$

Such a hamiltonian is generally called the Extended Bose-Hubbard model (eBHM). The analysis that follows will apply for any microscopic interactions that are long-range in nature to justify considering the nearest neighbour interactions, and not just those that have a dipolar origin. The details only become relevant if we wish to compute experimentally achievable values of V (as in Sec. 3.3). However, we will not be dealing with this in the thesis.

We are specifically interested in the case when $U, V > 0$. In such a situation, the on-site and nearest neighbour interactions compete with each other, introducing the possibility of breaking the translational symmetry. We proceed now to study how this affects the ground-state phases through a mean-field analysis.

4.1 Mean Field Theory

The mean-field decoupling of the eBHM largely proceeds the same way as with the BHM. The key difference is that we also need to decouple the $n_i n_j$ term by introducing another set of mean-field parameters, $\{\rho_i\}$.

$$\begin{aligned} \hat{a}_i &= \Psi_i + \delta\hat{a}_i & \hat{n}_i &= \rho_i + \delta\hat{n}_i \\ \implies \delta a_i^\dagger \delta a_j &= (a_i^\dagger - \Psi_i^*)(a_j - \Psi_j) \approx 0 & \implies \delta n_i \delta n_j &= (n_i - \rho_i)(n_j - \rho_j) \approx 0 \\ \implies a_i^\dagger a_j &\approx \Psi_j a_i^\dagger + \Psi_i^* a_j - \Psi_i^* \Psi_j & \implies n_i n_j &\approx \rho_j n_i + \rho_i n_j - \rho_i \rho_j \end{aligned} \quad (4.2)$$

Note here that since $n_i = a_i^\dagger a_i$, we could have simply used the first decoupling for the $n_i n_j$ term as well. However, the resulting mean-field hamiltonian turns out to be incapable of

hosting the phases we are interested in. In any case, neglecting the terms of $\mathcal{O}(\delta a_i^2)$ is a lower order approximation than neglecting $\mathcal{O}(\delta n_i^2)$.

Proceeding with the derivation, we already know the decoupling for the hopping term from Eq. (4.9). The decoupling for the interaction term proceeds in a similar way.

$$\begin{aligned} H_{int}/(V/2) &= \sum_{\langle i,j \rangle} n_i n_j \\ &= \sum_{\langle i,j \rangle} (\rho_j n_i + \rho_i n_j - \rho_i \rho_j) \\ &= \sum_i \left(\sum_{j \in N_i} \rho_j \right) n_i + \sum_i \left(\sum_{j \in N_i} \rho_j \right) n_i - \sum_i \left(\sum_{j \in N_i} \rho_j \right) \rho_i \end{aligned} \quad (4.3)$$

Defining the mean order parameter, $\bar{\rho}_i = \frac{1}{z} \sum_{j \in N_i} \rho_j$, we obtain the interaction term at the mean-field level.

$$H_{int}/(zV/2) = \sum_i (2\bar{\rho}_i n_i - \bar{\rho}_i \rho_i) \quad (4.4)$$

We can then write the entire site-decoupled hamiltonian which depends on a set of $2M$ mean-field parameters, $\{\Psi_i, \rho_i\}$.

$$H_i\{\Psi_i, \rho_i\} = -zt(\bar{\Psi}_i a_i^\dagger + \bar{\Psi}_i^* a_i - \bar{\Psi}_i \Psi_i^*) + \frac{zV}{2}(2\bar{\rho}_i n_i - \bar{\rho}_i \rho_i) + \frac{U}{2}n_i(n_i - 1) - \mu n_i \quad (4.5)$$

Following the derivation in Sec. 4.2, we might now be tempted to set $\Psi_i = \Psi$ and $\rho_i = \rho$. However, this is a bad choice to make for the eBHM, because as mentioned earlier, the interplay of the interaction terms allows the possibility of breaking the translational symmetry. Making this assumption would incorrectly ignore the existence of certain phases and misrepresent the extents of others. Instead, we can consider arbitrary periodic patterns across the lattice and write the mean-field hamiltonian for a single unit-cell as follows.

$$\begin{aligned} H_{MF,UC} &= \sum_{X \in UC} \left[-zt(\bar{\Psi}_X a_X^\dagger + \bar{\Psi}_X^* a_X) + (zV\bar{\rho}_X - \mu)n_X + \frac{U}{2}n_X(n_X - 1) \right] \\ &\quad - \sum_{X \in UC} \left[zt\bar{\Psi}_X \Psi_X^* - \frac{zV}{2}\bar{\rho}_X \rho_X \right] \end{aligned} \quad (4.6)$$

4.2 Analysis

4.2.1 1D lattice

Since the interaction term only acts between nearest neighbour pairs, there is only one periodic pattern that is possible for the 1D lattice. This simply comprises of a unit cell with two sites A and B that repeat through the lattice. It is prudent now to introduce the notion of a connectivity matrix that uniquely specifies the unit cell:

$$M_{UC} = \begin{pmatrix} A & B \\ A & B \end{pmatrix}$$



Such a matrix is always symmetric and is equivalent to representing the lattice as an undirected graph. Although this is not strictly required for the 1D chain, we will find it useful to distinguish different patterns in more complicated lattice geometries. The connectivity matrix also gives us a succinct way to compute the mean-field parameters.

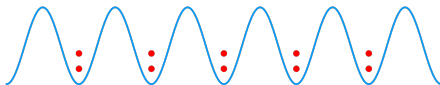
$$\begin{pmatrix} \bar{\Psi}_A \\ \bar{\Psi}_B \end{pmatrix} = M_{UC} \begin{pmatrix} \Psi_A \\ \Psi_B \end{pmatrix} \quad (4.7)$$

which in this case simply gives us $\bar{\Psi}_A = 2\Psi_B$ and $\bar{\Psi}_B = 2\Psi_A$. The same relation also holds for $\bar{\rho}_X$ and ρ_X . We can now construct the hamiltonian and self-consistently diagonalize it to obtain the ground state solution.

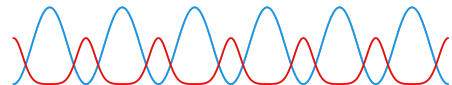
Classifying the phases

Note that we now have four mean-field parameters, $\{\Psi_A, \Psi_B, \rho_A, \rho_B\}$ and the various phases can be classified using them as follows.

- When $\rho_A = \rho_B = \rho$ and $\Psi_A = \Psi_B = \Psi$, this effectively restores translational invariance and describes a Mott Insulator when $\Psi = 0$ and a Superfluid otherwise.



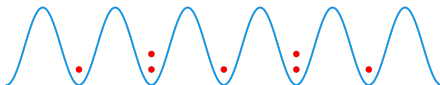
(a) Mott insulator



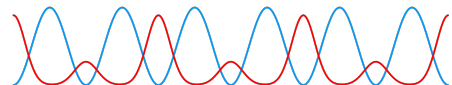
(b) Super-fluid

Figure 4.1: Pictorial representation of the BHM phases

- When $\rho_A \neq \rho_B$, this indicates a modulation of the average density of particles over the lattice and describes a Density Wave when $\Psi_A = \Psi_B = 0$ and a Supersolid otherwise.



(a) Density Wave



(b) Super-solid

Figure 4.2: Pictorial representation of the eBHM phases

It is not surprising that the eBHM also hosts Mott insulator and superfluid phases since the BHM can be recovered in the limit $V \rightarrow 0$. When we have $V \sim U$, however, two new analogous phases are introduced due to density modulations. The density wave phase can simply be interpreted as two inter-weaving Mott insulators with different occupation numbers. On the other hand, the supersolid can naively be described as a phase that exhibits superflow while also having some level of crystalline order due to the periodic density modulations. Such an interpretation is rather imprecise and has been the topic of numerous debates, but the nature of the phase is fairly clear atleast at the mean-field level.

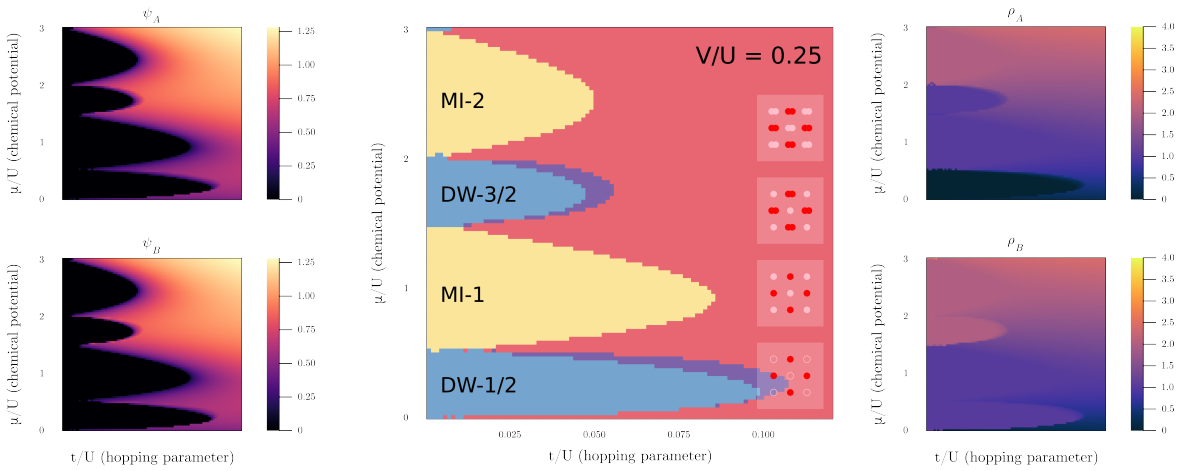


Figure 4.3: Mean-field phase diagram of 1D lattice

We can see from Fig. 5.3 that for an intermediate value of V/U , all four phases can exist in the $t - \mu$ plane. The density wave seems to appear as lobes in a similar manner to the Mott insulator. Peculiarly, the supersolid phase is only ever observed at the ‘edges’ of these density wave lobes. Consequently, there is no possibility of finding a phase transition directly from the density wave to the superfluid phase. Similarly, there is no direct transition from a Mott insulator to a supersolid. This seems to support the fact that a quantum phase transition can only occur if it involves breaking a single symmetry of the system.

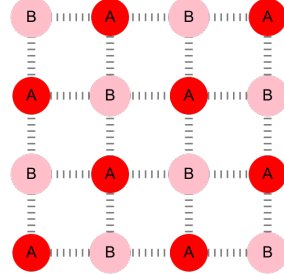
We also note that we can label the density wave lobes with their average filling just as we differentiated Mott insulator lobes with their occupation number. However, this does not uniquely identify them, since a density wave having a filling of $(1, 2)$ and $(0, 3)$ will both have an average occupation of $3/2$ as seen in Fig. 5.4.

4.2.2 2D square lattice

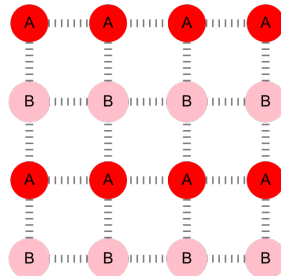
For a square lattice, we can come up with more than one possible repeating unit cell that breaks translational symmetry. In such a case, we must find the solution in either case and

only admit the one having lowest ground state energy.

$$M_{UC} = \begin{matrix} & A & B \\ A & 0 & 4 \\ B & 4 & 0 \end{matrix}$$



$$M_{UC} = \begin{matrix} & A & B \\ A & 2 & 2 \\ B & 2 & 2 \end{matrix}$$



It turns out that the first pattern satisfies this condition for all parameter regimes of interest. We see in Fig. 5.4 that the phase diagram for a 2D square lattice qualitatively looks similar to that of the 1D lattice in Fig. 5.3. This is because the connectivity matrix of the dominant pattern in either case is only different by a scaling factor of two. We also note that as V/U is increased, the density wave lobes arise between Mott insulator lobes and increase in extent until the latter becomes unstable in the $t - \mu$ plane. Also note that the density waves become the dominant phase in the diagram roughly when $zV \sim U$ as one would expect.

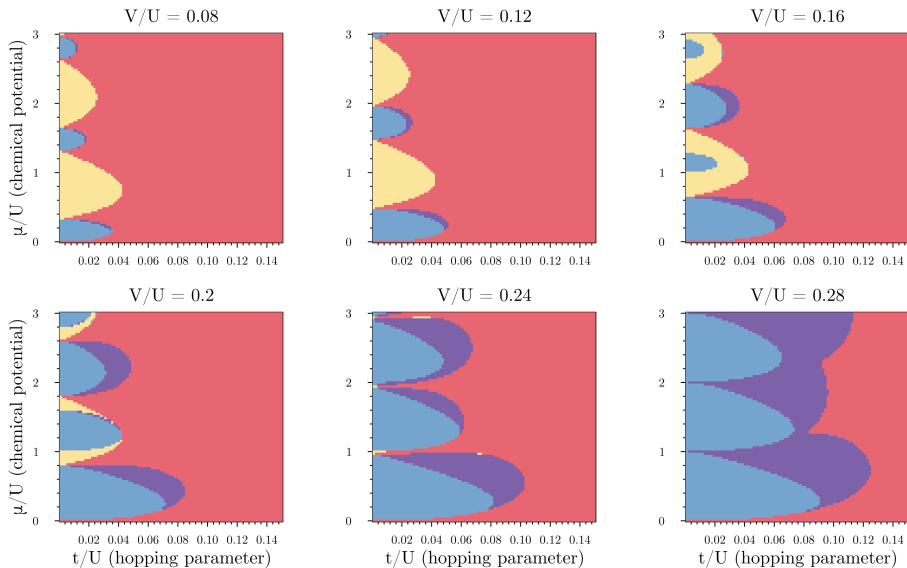
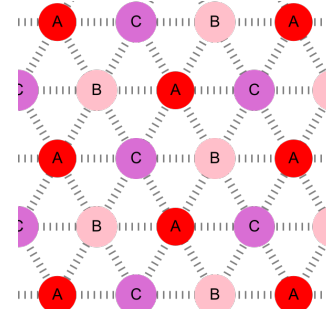


Figure 4.4: Mean-field phase diagram of 2D square lattice

4.2.3 2D triangular lattice

We consider the following sub-lattice pattern for our analysis of the triangular lattice.

$$M_{UC} = \begin{pmatrix} A & B & C \\ A & 0 & 3 & 3 \\ B & 3 & 0 & 3 \\ C & 3 & 3 & 0 \end{pmatrix}$$



We can see in Fig. 5.5 that the phase diagram has some qualitative differences to that of the square lattice. There are now two density wave lobes between each pair of mott insulator lobes due to the additional fractional fillings of the triangular lattice (i.e. 1/3, 2/3, etc).

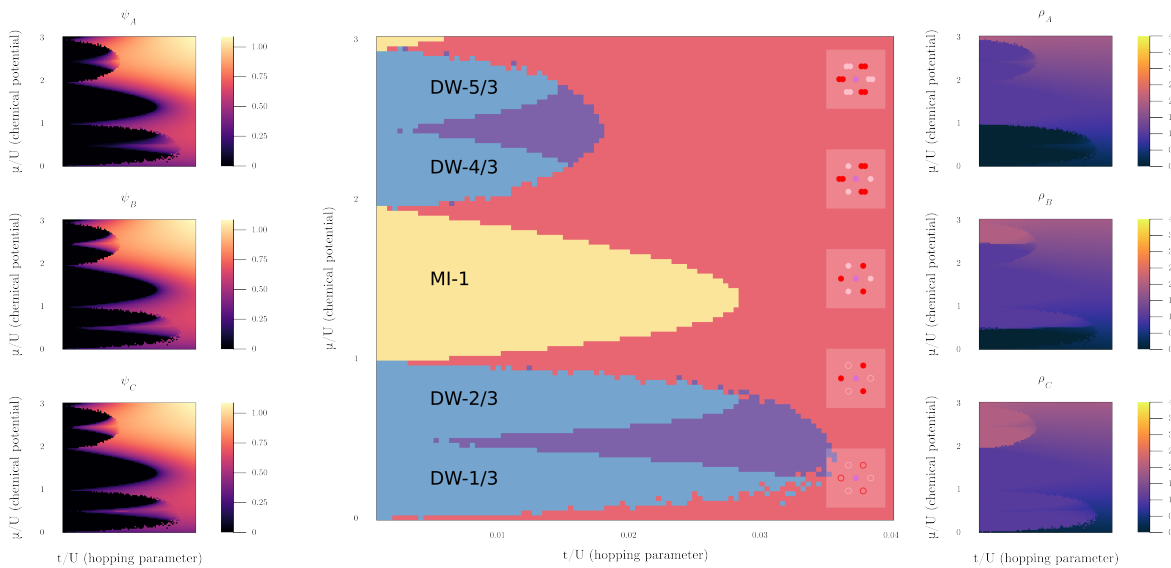


Figure 4.5: Mean-field phase diagram of triangular lattice

4.3 Caveats w/ self-consistency

When we introduced the idea of self-consistency in Chapter 4, we also described the procedure in terms of finding the fixed point of a function. This holds true for the eBHM as well, except the function is now multi-variate which significantly complicates things.

For instance, our naive decision to utilize Fixed Point iteration without evaluating the conditions required for convergence has finally caught up with us.

Unfortunately, the order parameters are generally related in a highly non-linear way which makes it hard to determine these conditions analytically. Instead, below are the problems that were encountered while numerically solving the system, along with possible solutions to mitigate them.

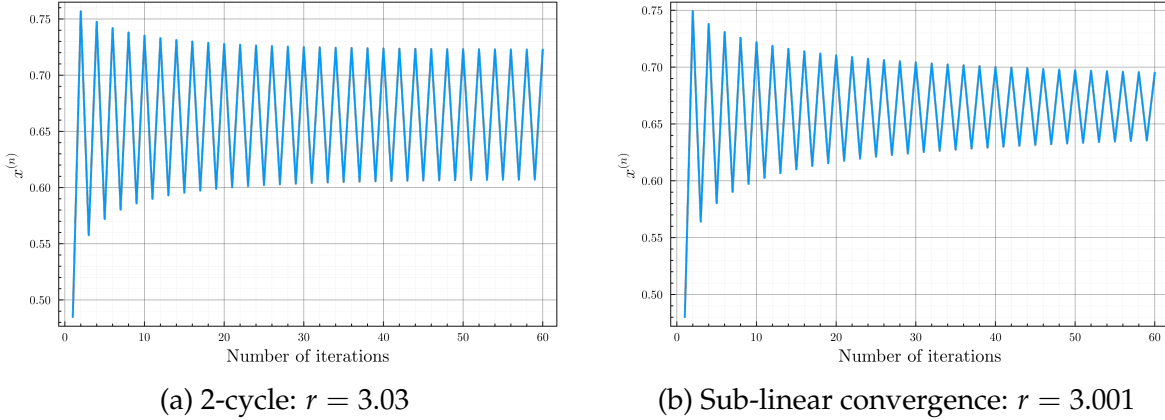


Figure 4.6: Convergence issues demonstrated using logistic map, $x^{(n+1)} = rx^{(n)}(1 - x^{(n)})$

4.3.1 No convergence

This generally manifests in the form of 2-cycles.

$$\begin{aligned} f(\{\Psi_A, \Psi_B, \rho_A, \rho_B\}) &= \{\Psi'_A, \Psi'_B, \rho'_A, \rho'_B\} \\ f(\{\Psi'_A, \Psi'_B, \rho'_A, \rho'_B\}) &= \{\Psi_A, \Psi_B, \rho_A, \rho_B\} \end{aligned}$$

Every 2-cycle encountered also seems to have a pattern that can be exploited to guess the actual fixed point. For example:

$$\begin{aligned} \textbf{2-cycle: } & (\Psi_A, \Psi_B, \rho_1, \rho_2) \rightarrow (\Psi_A, \Psi_B, \rho_2, \rho_1) \\ \textbf{Fixed point: } & (\Psi_A, \Psi_B, (\rho_1 + \rho_2)/2, (\rho_1 + \rho_2)/2) \end{aligned}$$

Several patterns like this can emerge, and one solution is to hard-code the guesses for fixed points for each case. This is unfortunately not scalable to arbitrary lattice geometries and parameter regimes. This problem arises from the strong dependancy on the initial guess for the self-consistency loop, and can be remedied by taking several initial guesses till one of them converges.

4.3.2 Sub-linear convergence

This manifests in a form that is decievingly similar to a 2-cycle.

$$f(\{\Psi_A, \Psi_B, \rho_A, \rho_B\}) \approx \{\Psi'_A, \Psi'_B, \rho'_A, \rho'_B\}$$

$$f(\{\Psi'_A, \Psi'_B, \rho'_A, \rho'_B\}) \approx \{\Psi_A, \Psi_B, \rho_A, \rho_B\}$$

The convergence happens at a very slow rate, especially close to the phase boundaries. This can be handled by utilizing techniques that are more advanced than fixed point iteration such as Nesterov's acceleration.

4.3.3 Local minima

Finally, we come to an important point that there may be several stable fixed points for the same system. By nature of the formulation of the mean-field technique, the true solution is the one with the lowest ground state energy. As a result, one is forced to perform self-consistency starting with a variety of initial guesses to avoid falling into local minima. There does not seem to be a simple way to sample the parameter space in an efficient manner to generate initial guesses. So, an arbitrarily chosen uniform grid was utilized for the results presented in this thesis, but this solution is hardly satisfactory.

CHAPTER

5

Spinful bosons in a lattice

In this chapter, we explore the nature of another form of short-ranged interaction, this time induced by spin-spin coupling. For this purpose, we will consider the simplest modification of the spinless case, which is the spin-1 Bose Hubbard model.

$$H = -t \sum_{\langle i,j \rangle \sigma} a_{i\sigma}^\dagger a_{j\sigma} + \frac{U}{2} \sum_i n_i(n_i - 1) + V_s \sum_i (S_i^2 - 2n_i) - \mu \sum_i n_i \quad (5.1)$$

The spin operators are determined as shown below, using the spin-1 matrices, $\{J_x, J_y, J_z\}$.

$$J_x = \frac{1}{\sqrt{2}} \begin{pmatrix} 0 & 1 & 0 \\ 1 & 0 & 1 \\ 0 & 1 & 0 \end{pmatrix} \quad J_y = \frac{i}{\sqrt{2}} \begin{pmatrix} 0 & -1 & 0 \\ 1 & 0 & -1 \\ 0 & 1 & 0 \end{pmatrix} \quad J_z = \begin{pmatrix} 1 & 0 & 0 \\ 0 & 0 & 0 \\ 0 & 0 & -1 \end{pmatrix} \quad (5.2)$$

$$\vec{S}_i = \sum_{\alpha\beta} a_{i\alpha}^\dagger \vec{J}_{\alpha\beta} a_{i\beta} \quad (5.3)$$

Note that we have only taken into account the on-site interactions (due to contact scattering and spin-spin coupling). As a result, we do not expect to observe any fundamentally new phases besides the mott insulator and superfluid. However, now that the bosons have an extra degree of freedom due to their spin ($S = 1, m_s \in \{1, 0, -1\}$), we expect these phases to also have magnetic ordering.

5.1 Mean Field Theory

The mean-field decoupling for the spin-1 BHM is quite similar as for the spinless BHM since we have only introduced additional on-site interaction terms. However, we are now forced to introduce three mean-field parameters for each lattice site, one for each spin projection, $\hat{a}_{i\sigma} = \Psi_{i\sigma} + \delta\hat{a}_{i\sigma}$, where $\sigma \in \{1, 0, -1\}$. This gives us the decomposition of the hopping hamiltonian as follows.

$$-H_{hop}/zt = \sum_{i\sigma} (\bar{\Psi}_{i\sigma} a_{i\sigma}^\dagger + \bar{\Psi}_{i\sigma}^* a_{i\sigma} - \bar{\Psi}_{i\sigma} \Psi_{i\sigma}^*) \quad (5.4)$$

As usual, we can assume translational invariance in the ground state and set $\Psi_{i\sigma} = \Psi_\sigma \forall i$. We will also set $\Psi_\sigma \in \mathbb{R}$ for now, but will revisit this assumption further below. The spin-1

BHM can now be written as a sum over single-site hamiltonians.

$$H_i\{\Psi_{i\sigma}\} = -zt \sum_{\sigma} (\Psi_{i\sigma} a_{i\sigma}^{\dagger} + \Psi_{i\sigma}^* a_{i\sigma} - \Psi_{i\sigma} \Psi_{i\sigma}^*) + \frac{U_s}{2} (S_i^2 - 2n_i) + \frac{U}{2} n_i(n_i - 1) - \mu n_i \quad (5.5)$$

The spin interaction term can be explicitly computed in terms of the creation/annihilation operators as shown below (where we have introduced the spin index $\bar{1}$ instead of -1 for notational clarity).

$$\begin{pmatrix} S_x \\ S_y \\ S_z \end{pmatrix} = \begin{pmatrix} \frac{1}{\sqrt{2}}(a_{i1}^{\dagger}a_{i0} + a_{i0}^{\dagger}a_{i1} + a_{i\bar{1}}^{\dagger}a_{i0} + a_{i0}^{\dagger}a_{i\bar{1}}) \\ \frac{i}{\sqrt{2}}(-a_{i1}^{\dagger}a_{i0} + a_{i0}^{\dagger}a_{i1} + a_{i\bar{1}}^{\dagger}a_{i0} - a_{i0}^{\dagger}a_{i\bar{1}}) \\ n_{i1} - n_{i\bar{1}} \end{pmatrix} \quad (5.6)$$

$$S_i^2 = 2n_{i1}n_{i0} + 2n_{i0}n_{i\bar{1}} - 2n_{i1}n_{i\bar{1}} + n_{i1} + 2n_{i0} + n_{i\bar{1}} + n_{i1}^2 + n_{i\bar{1}}^2 + 2a_{i1}^{\dagger}a_{i\bar{1}}^{\dagger}a_{i0}^2 + 2(a_{i0}^{\dagger})^2a_{i1}a_{i\bar{1}} \quad (5.7)$$

Note that most of the terms in the S_i^2 operator are block-diagonal in the spin subspaces except for the last two terms which mix the spin components. We can now construct the mean-field hamiltonian in the occupation basis, $|n_1, n_0, n_{\bar{1}}\rangle$ resulting in the following ansatz for the wavefunction.

$$|\Psi\rangle = \bigotimes_{i=1}^M \left(\sum_{n_1, n_0, n_{\bar{1}}} f_{i, n_1, n_0, n_{\bar{1}}} |n_1, n_0, n_{\bar{1}}\rangle \right) \quad (5.8)$$

5.1.1 Mott insulator phase

When the order parameters satisfy $\Psi_1 = \Psi_0 = \Psi_{\bar{1}} = 0$, the ground state is a Mott insulator. In this section, we will try to understand the nature of the Mott insulator lobes due to the spin degree of freedom, by considering the hamiltonian in the limit $t \ll U$.

$$H_i = \frac{U_s}{2} (S_i^2 - 2n_i) + \frac{U}{2} n_i(n_i - 1) - \mu n_i \quad (5.9)$$

The ground state would clearly be a fock state with a fixed total occupation number, n_i such that it is a superposition of spin states ($\sum_{\sigma} n_{i\sigma} = n_i$). However, note that S_i^2 , S_{iz} and n_i commute with each other. As a result, a better basis for our analysis is the combined spin basis, $|n_i; S_i, m_i\rangle$ which is defined by the following eigenvalue equations.

$$\hat{S}_i^2 |n_i; S_i, m_i\rangle = S_i(S_i + 1) |n_i; S_i, m_i\rangle \quad (5.10)$$

$$\hat{S}_{iz} |n_i; S_i, m_i\rangle = m_i |n_i; S_i, m_i\rangle \quad (5.11)$$

$$\hat{n}_i |n_i; S_i, m_i\rangle = n_i |n_i; S_i, m_i\rangle \quad (5.12)$$

We can then write the ground state energy for the state $|n; S, m\rangle$ as follows:

$$E(S, n) = \frac{U_s}{2} (S(S + 1) - 2n) + \frac{U}{2} n(n + 1) - \mu n \quad (5.13)$$

Before we can determine the state $|n; S, m\rangle$, we must discuss the constraints on these quantum numbers. To begin with, we write the form of the spin ladder operators.

$$S_+ = S_x + iS_y = \sqrt{2}(a_1^\dagger a_0 + a_0^\dagger a_{\bar{1}}) \quad S_- = S_x - iS_y = \sqrt{2}(a_0^\dagger a_1 + a_{\bar{1}}^\dagger a_0) \quad (5.14)$$

Since the spin operators obey the $SU(2)$ commutation relations, $[S_{i\alpha}, S_{j\beta}] = i\epsilon_{\alpha\beta\gamma}S_{i\gamma}$, the ladder structure follows and we have $m \in \{0, \pm 1, \pm 2, \dots \pm S\}$, generating $2S + 1$ states for a given value of n and S . Let us now consider the state $|n; S, -S\rangle$ to determine the allowed values of S . Applying S_z on this state gives us the following relations:

$$2n_1 = (n - S) - n_0 \quad (5.15)$$

$$2n_{\bar{1}} = (n + S) - n_0 \quad (5.16)$$

This tells us that $S \leq n$ and further, $(n + S)$ and n_0 must both either be even or odd. If we assume that they are odd, we can expand the state $|n; S, -S\rangle$ in the following way.

$$|\Psi\rangle = |n; S, -S\rangle = \sum_{n_0} c_{n_0} \left| n_0, \frac{n - n_0 + S}{2}, \frac{n - n_0 - S}{2} \right\rangle = \sum_{n_0} c_{n_0} |\Psi_{n_0}\rangle \quad (5.17)$$

By construction, we know that $S_- |\Psi\rangle = 0$. However, note that the first term $S_- |\Psi_1\rangle$ gives rise to a state having $n_0 = 0$ since $S_- \sim a_{\bar{1}}^\dagger a_0$. No other term arising from $S_- |\Psi_i\rangle$ for odd $i \geq 3$ can generate such a state with $n_0 = 0$. Since the overall result must vanish, we conclude that $c_1 = 0$. Similarly, by considering the subsequent terms, we can argue that $c_i = 0 \forall i$. As a result, $S_- |\Psi\rangle = 0 \implies |\Psi\rangle = 0$, but we know that $|n; S, -S\rangle \neq 0$ so $(N + L)$ cannot be odd. Such an argument fails when n_0 is even, since we can conclude $c_i = 0 \forall i \geq 2$ but the lowest order term vanishes under annihilation, so c_0 can be non-zero. Thus, we have the constraint that $(n + S)$ must be even. This means that if n is even, $S \in \{0, 2, 4, \dots, n\}$ and if n is odd, $S \in \{1, 3, 5, \dots, n\}$. We will see in the subsequent sections that this constraint directly affects the ground state and hence the phase diagram.

5.1.2 Superfluid phase

To characterize the superfluid phase, we turn our attention to the set of mean-field parameters which can be grouped like so, $\Psi = (\Psi_1, \Psi_0, \Psi_{\bar{1}}) = \sqrt{n_s}(\eta_1, \eta_0, \eta_{\bar{1}})$, where $n_s = |\Psi|$ is the superfluid density and η is a normalized spinor. Naturally, when n_s does not vanish, we observe a superfluid phase and can understand its magnetic properties using the average spin given by $\langle S \rangle = \sum_{\alpha\beta} \eta_\alpha^* J_{\alpha\beta} \eta_\beta$. Writing out the components, we get:

$$\begin{pmatrix} \langle S_x \rangle \\ \langle S_y \rangle \\ \langle S_z \rangle \end{pmatrix} = \begin{pmatrix} \sqrt{2}(\eta_1 \eta_0 + \eta_{\bar{1}} \eta_0) \\ 0 \\ \eta_1^2 - \eta_{\bar{1}}^2 \end{pmatrix} \quad (5.18)$$

Notice that the y -component of the average spin vanishes. At this point, we must review our assumption that $\Psi_\sigma \in \mathbb{R}$. Generally, this is valid because the BHM is invariant under

the $U(1)$ transformation, $a_i \rightarrow e^{i\theta} a_i$ and any phase carried by the order parameter, Ψ , can be shifted onto the operators. However, in the spin-1 case, we would like to set all three order parameters, Ψ_σ to be real.

This creates an issue since the BHM is only invariant under *global* gauge transformations, whereas our order parameters might carry different phases for each spin component, resulting in the transformation $a_{i\sigma} \rightarrow e^{i\theta_\sigma} a_{i\sigma}$. It can be seen that the spin-1 BHM is invariant under such a transformation only if $\theta_1 + \theta_{-1} - 2\theta_0 = m\pi$ where $m \in \mathbb{Z}$, precisely due to the spin mixing components of S^2 . We can still set $\Psi_\sigma \in \mathbb{R}$ but this manifests in constraining the spin components of the superfluid strictly to the $x - z$ plane. While this means that we have lost generality, the physics of the system still remains the same and we will continue with this assumption for the sake of simplicity.

Getting back to the average spin, a nicer quantity to work with is its magnitude squared.

$$\begin{aligned}
|\langle S \rangle|^2 &= 2(\eta_1\eta_0 + \eta_{-1}\eta_0)^2 + (\eta_1^2 - \eta_{-1}^2)^2 \\
&= 2(\eta_1^2\eta_0^2 + \eta_{-1}^2\eta_0^2 + 2\eta_0^2\eta_1\eta_{-1}) + \eta_1^4 + \eta_{-1}^4 - 2\eta_1^2\eta_{-1}^2 \\
&= (1 - \eta_0^2)\eta_0^2 + (1 - (\eta_1^2 + \eta_{-1}^2))(\eta_1^2 + \eta_{-1}^2) + 4z^2\eta_1\eta_{-1} + \eta_1^4 + \eta_{-1}^4 - 2\eta_1^2\eta_{-1}^2 \\
&= \eta_0^2 - \eta_0^4 + \eta_1^2 + \eta_{-1}^2 - (\eta_1^2 + \eta_{-1}^2)^2 + 4\eta_0^2\eta_1\eta_{-1} + \eta_1^4 + \eta_{-1}^4 - 2\eta_1^2\eta_{-1}^2 \\
&= 1 - \eta_0^4 + 4\eta_0^2\eta_1\eta_{-1} - 4\eta_1^2\eta_{-1}^2 \\
&= (1 - (\eta_0^2 - \eta_1\eta_{-1})^2)
\end{aligned} \tag{5.19}$$

If we define the singlet operator as $\Theta_i = (a_{i0}^2 - 2a_{i1}a_{i-1})$, we can directly relate its expectation value to the average spin like so $|\langle S \rangle|^2 = 1 - |\langle \Theta \rangle|^2/n_s^2$. In the ground state, based on the sign of U_s , the energy is minimized by $|\langle S \rangle|^2 = 0$ or $|\langle S \rangle|^2 = 1$ corresponding to a 'polar' or 'ferro' superfluid respectively.

5.2 Results

5.2.1 Ferromagnetic interactions ($U_s < 0$)

In this case, the energy is minimized when all the bosons are in the same spin state. As a result, the superfluid is of 'ferro' nature and exhibits average spin $|\langle S \rangle|^2 = 1$. Similarly, in the Mott insulator phase, each site has a net spin of $S = N$, where N is the number of bosons occupying the site in that Mott lobe. This is allowed by the constraint we obtained in Sec. 6.1.1. As a result, there is no qualitative difference in the phase boundaries as compared to the spinless case. Note that whenever we mention 'spin', we mean the quantum number S and not the projection m_s . As a result, in the absence of an external magnetic field, the system is magnetically unordered. We see that the observations discussed here are in agreement with Fig. 6.1.

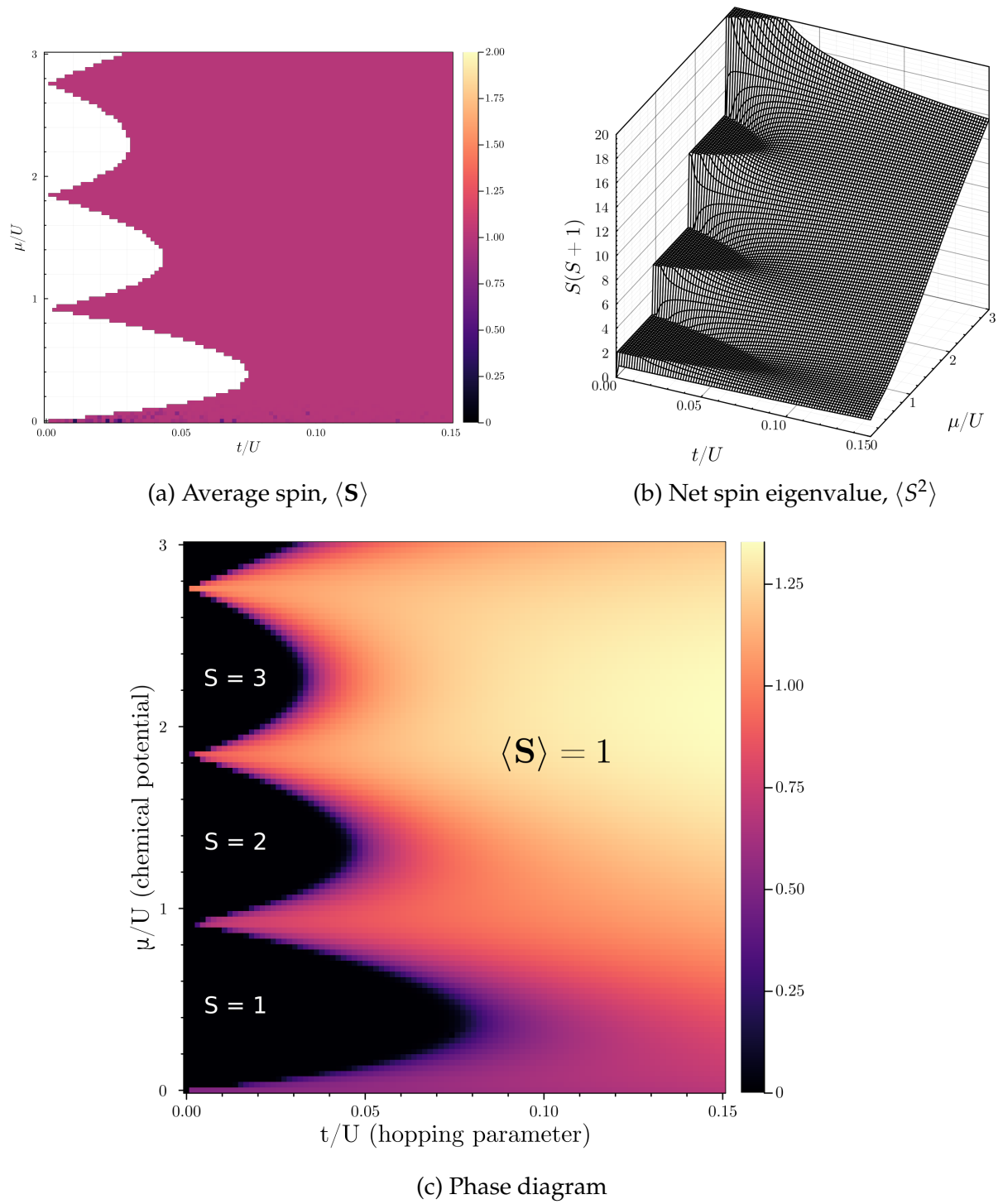


Figure 5.1: Ferromagnetic interactions, $U_s = -0.08U$

5.2.2 Anti-ferromagnetic interactions ($U_s > 0$)

In this case, the energy is minimized when the net spin of the bosons vanishes. As a result, the superfluid is of ‘polar’ nature and exhibits average spin $|\langle S \rangle|^2 = 0$. Things get interesting in the Mott insulator phase, however, since the constraint from Sec. 6.1.1 plays a bigger role now as we can see in Fig. 6.2.

The Mott lobes with even N is described by the state $|N; 0, 0\rangle$ with $N/2$ pairs of spin singlets, whereas the Mott lobes with odd N is described by the state $|N; 1, m\rangle$ such that there is one boson that cannot form a singlet. This has a direct effect on the phase boundaries since singlet formation stabilizes the Mott insulator against the superfluid transition. As a result, there is significant difference in the phase boundary of this system as compared to the spinless case. Further, note that the SF-MI transition is generally second order in nature. However, in this case, only the SF-(odd) MI transitions are second order, while the SF-(even) MI transitions are first order in nature.

5.3 Effective spin-spin interactions

While the mean-field decoupling allowed us to study the effect of the spin degree of freedom on the ordered phases of the BHM, it also threw away any correlations across the lattice. In the pure mott insulator limit when $t \ll U$, such a treatment is accurate since the orientations of spins in different lattice sites are genuinely uncorrelated. However, as we introduce finite hopping, the bosons can mediate an interaction between the spins on different sites, thus introducing spin-spin correlations that can give rise to singlet and nematic ordering within the mott lobes.

In general, one can write an effective spin hamiltonian for such a case.

$$H_{\text{eff}} = \sum_{\langle i,j \rangle} (-J_{i,j}^{(0)} - J_{i,j}^{(1)} S_i \cdot S_j - J_{i,j}^{(2)} (S_i \cdot S_j)^2) \quad (5.20)$$

where the coefficients are determined by a perturbative treatment of the hopping term. However, we will not pursue this exercise here since the phenomenon of mediation is complicated by the presence of the other terms in the spin-1 BHM. Instead, we study a simpler situation that demonstrates mediation more clearly in the next chapter.

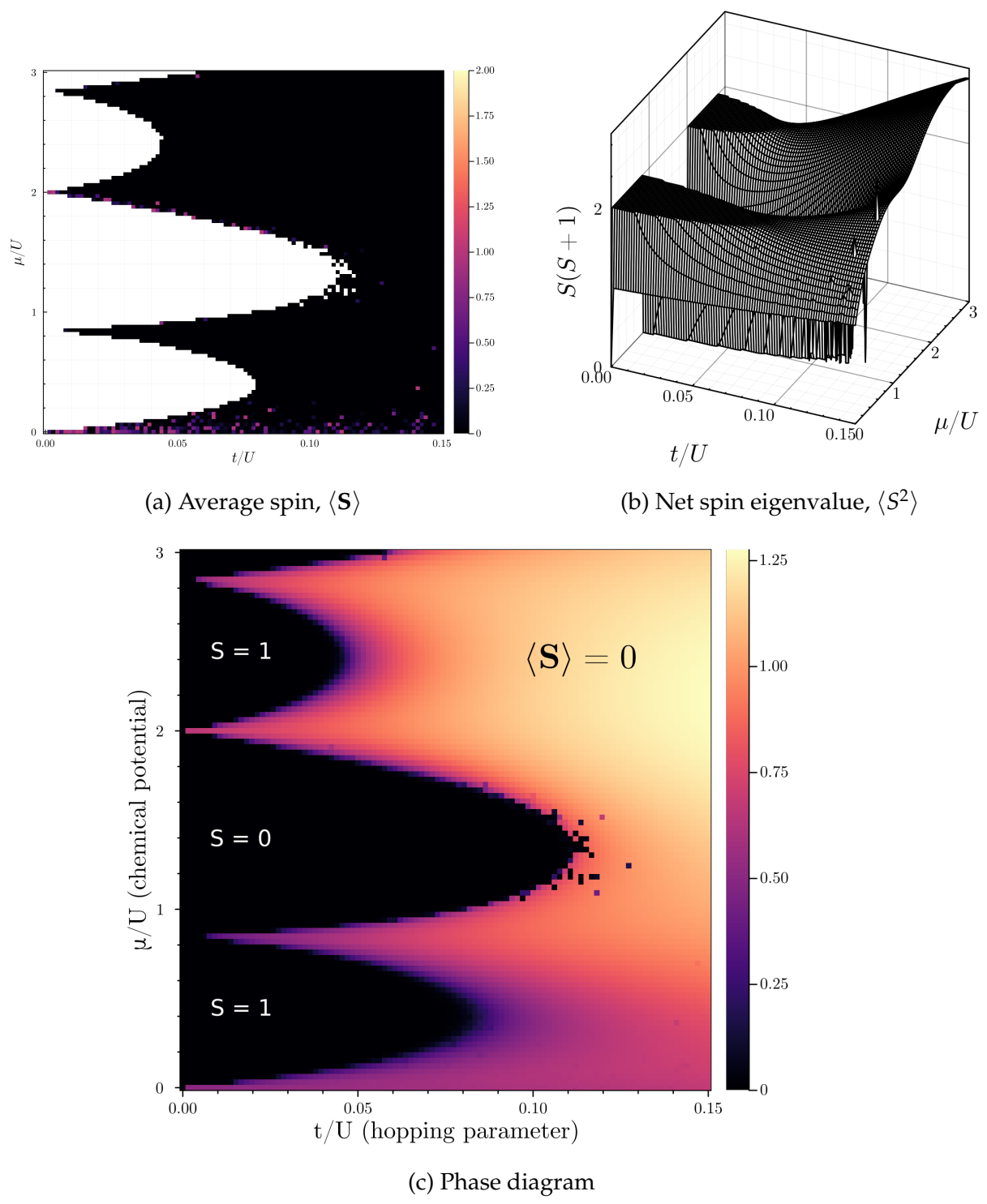


Figure 5.2: Anti-ferromagnetic interaction, $U_s = 0.08U$

CHAPTER

6

Boson-mediated interactions

In this chapter, we consider a simple model of non-interacting spin-1 bosons on a lattice coupled with a lattice of localized spin-1 bosonic ‘impurities’. This can be seen as analogue of the fermionic lattice kondo model. Our goal is to explore the nature boson-mediated interactions.

$$H = -t \sum_{\langle i,j \rangle, \sigma} a_{i\sigma}^\dagger a_{j\sigma} - J_h \sum_i S_i \cdot s_i \quad (6.1)$$

This model can be thought of arising from a more general one involving coupling between the lattice and impurity bosons, in the limit of single particle occupation in the impurity sites. As a result, the localized spins can be treated as classical spins such that $|\vec{S}_i| = 1$, parametrized like so $\vec{S}_i = (\cos \phi_i \sin \theta_i, \sin \phi_i \sin \theta_i, \cos \theta_i)$. Note that the localized spins do not directly interact with each other in this hamiltonian.

6.1 Strong-coupling limit

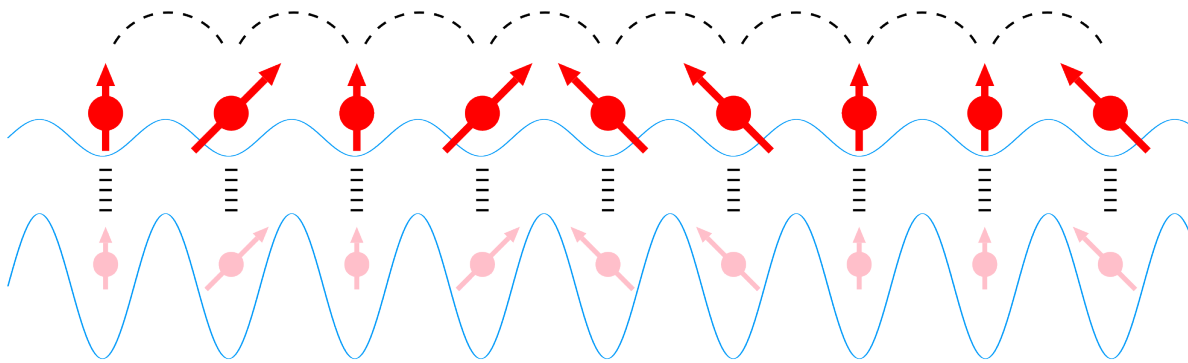


Figure 6.1: Conduction bosons (red) and impurity bosons (pink) confined in a lattice

Let us consider the limit $J_h \gg t$ wherein the bosons have a strong tendency to align with the classical spins. This motivates us to change our basis by applying a site-dependant $SU(2)$ rotation:

$$\begin{bmatrix} a_{i,1} \\ a_{i,0} \\ a_{i,\bar{1}} \end{bmatrix} = \begin{bmatrix} \cos^2 \frac{\theta_i}{2} & -\frac{1}{\sqrt{2}} \sin \theta_i e^{-i\phi_i} & \sin^2 \frac{\theta_i}{2} e^{-2i\phi_i} \\ \frac{1}{\sqrt{2}} \sin \theta_i e^{i\phi_i} & \cos \theta_i & -\frac{1}{\sqrt{2}} \sin \theta_i e^{-i\phi_i} \\ \sin^2 \frac{\theta_i}{2} e^{2i\phi_i} & \frac{1}{\sqrt{2}} \sin \theta_i e^{i\phi_i} & \cos^2 \frac{\theta_i}{2} \end{bmatrix} \begin{bmatrix} d_{i,1} \\ d_{i,0} \\ d_{i,\bar{1}} \end{bmatrix} \quad (6.2)$$

The new operators $d_{i,\sigma}$ annihilates a boson at site i with the spin $\sigma \in [1, 0, \bar{1}]$ such that the quantization axis is now parallel to the localized spin. The transformed hamiltonian now looks as follows:

$$H = \underbrace{\sum_{\langle i,j \rangle \sigma\sigma'} g_{ij}^{\sigma\sigma'} d_{i\sigma}^\dagger d_{i\sigma'}}_V - \underbrace{J_H \sum_i (n_{i,1} - n_{i,\bar{1}})}_{H_0} \quad (6.3)$$

where $n_{i,\sigma}$ are the defined by $d_{i,\sigma}^\dagger d_{i,\sigma}$. Note that this transformation effectively diagonalizes the spin coupling term, which allows us to treat the hopping term in a perturbative manner. Although the elements of the new hopping matrix are not particularly insightful, they are listed below (as a multiple of $t_{i,j}$) for completeness.

$$\begin{aligned} g_{i,j}^{1,1} &= \cos^2 \frac{\theta_i}{2} \cos^2 \frac{\theta_j}{2} + \frac{1}{2} e^{-i(\phi_i - \phi_j)} \sin \theta_i \sin \theta_j + e^{-2i(\phi_i - \phi_j)} \sin^2 \frac{\theta_i}{2} \sin^2 \frac{\theta_j}{2} \\ g_{i,j}^{1,0} &= \frac{1}{\sqrt{2}} e^{-i\phi_i} \sin \theta_i \cos \theta_j - \frac{1}{\sqrt{2}} e^{-i\phi_j} \cos^2 \frac{\theta_i}{2} \sin \theta_j + \frac{1}{\sqrt{2}} e^{-i(2\phi_i - \phi_j)} \sin^2 \frac{\theta_i}{2} \sin \theta_j \\ g_{i,j}^{1,\bar{1}} &= e^{-2i\phi_i} \cos^2 \frac{\theta_j}{2} \sin^2 \frac{\theta_i}{2} + e^{-2i\phi_j} \cos^2 \frac{\theta_i}{2} \sin^2 \frac{\theta_j}{2} - \frac{1}{2} e^{-i(\phi_i + \phi_j)} \sin \theta_i \sin \theta_j \\ g_{i,j}^{0,0} &= \cos \theta_i \cos \theta_j + \frac{1}{2} e^{i(\phi_i - \phi_j)} \sin \theta_i \sin \theta_j + \frac{1}{2} e^{-i(\phi_i - \phi_j)} \sin \theta_i \sin \theta_j \\ g_{i,j}^{0,\bar{1}} &= \frac{1}{\sqrt{2}} e^{-i\phi_i} \cos^2 \frac{\theta_j}{2} \sin \theta_i - \frac{1}{\sqrt{2}} e^{-i\phi_j} \cos \theta_i \sin \theta_j - \frac{1}{\sqrt{2}} e^{-i(-\phi_i + 2\phi_j)} \sin \theta_i \sin^2 \frac{\theta_j}{2} \\ g_{i,j}^{\bar{1},\bar{1}} &= \cos^2 \frac{\theta_i}{2} \cos^2 \frac{\theta_j}{2} + \frac{1}{2} e^{i(\phi_i - \phi_j)} \sin \theta_i \sin \theta_j + e^{2i(\phi_i - \phi_j)} \sin^2 \frac{\theta_i}{2} \sin^2 \frac{\theta_j}{2} \end{aligned}$$

The remaining elements can be computed by using the property $g_{i,j}^{\sigma,\sigma'} = (g_{j,i}^{\sigma',\sigma})^*$. This result can be understood as the spin-coupling resulting in an effective hopping term as it inhibits the process. Let us now consider a simple case of unit occupation on the lattice, and further, we limit ourselves to a two-site problem. The ground state for the unperturbed system is triply degenerate:

$$|0,2\rangle = d_{2,2}^\dagger d_{2,1}^\dagger |0\rangle \quad |2,0\rangle = d_{1,1}^\dagger d_{1,1}^\dagger |0\rangle \quad |1,1\rangle = d_{2,1}^\dagger d_{1,1}^\dagger |0\rangle$$

with energy $E_0^{(0)} = -2J_h$. Since the ground state is degenerate, we must diagonalize V within this subspace to calculate the first order correction to the ground state energy. This involves the computation of vacuum expectation values like so:

$$g_{ii'}^{\sigma\sigma'} \langle 0 | d_{m'\beta'} d_{m\beta} d_{i\sigma}^\dagger d_{i'\sigma'} d_{l,\alpha}^\dagger d_{l',\alpha'}^\dagger | 0 \rangle = g_{m'l'}^{\beta'\alpha'} \delta_{lm} \delta_{\alpha\beta} + g_{m'l'}^{\beta'\alpha} \delta_{l'm} \delta_{\alpha'\beta} + g_{ml}^{\beta\alpha'} \delta_{lm'} \delta_{\alpha\beta'} + g_{ml}^{\beta\alpha} \delta_{l'm'} \delta_{\alpha'\beta'} \quad (6.4)$$

Details can be found in Appendix B. We can then compute the matrix V in the ground state subspace as follows.

$$V = 2 \operatorname{Re} \begin{pmatrix} g_{1,1}^{1,1} + g_{2,2}^{1,1} & 2g_{1,2}^{1,1} & 2g_{2,1}^{1,1} \\ 2g_{1,2}^{1,1} & 4t_{1,1}^{1,1} & 0 \\ 2g_{2,1}^{1,1} & 0 & 4g_{2,2}^{1,1} \end{pmatrix} = 4 \begin{pmatrix} 0 & \operatorname{Re}(g_{1,2}^{1,1}) & \operatorname{Re}((g_{1,2}^{1,1})^*) \\ \operatorname{Re}(g_{1,2}^{1,1}) & 0 & 0 \\ \operatorname{Re}((g_{1,2}^{1,1})^*) & 0 & 0 \end{pmatrix} \quad (6.5)$$

The smallest eigenvalue is the first order correction, $E_0^{(1)} = -4\sqrt{2}\operatorname{Re}(g_{1,2}^{1,1})$, giving us the following expression.

$$E_0^{(1)}(\theta_i, \phi_i, \theta_j, \phi_j) = -4\sqrt{2}t_{i,j} \left[\cos^2 \frac{\theta_i}{2} \cos^2 \frac{\theta_j}{2} + \frac{1}{2} \cos(\phi_i - \phi_j) \sin \theta_i \sin \theta_j + \cos(2(\phi_i - \phi_j)) \sin^2 \frac{\theta_i}{2} \sin^2 \frac{\theta_j}{2} \right] \quad (6.6)$$

Note that we have 'integrated out' the bosonic part of the system and have an expression for the corrected energy purely in terms of the localized spin components. Thus, we have $H_{\text{eff}}(\theta_i, \phi_i, \theta_j, \phi_j) = E_0^{(1)}(\theta_i, \phi_i, \theta_j, \phi_j) + E_0^{(0)}$ as an effective hamiltonian governing the physics of the localized spins. We can also clearly see that the two spin variables are coupled in a non-trivial manner, thereby acting as an effective interaction that is mediated by the lattice bosons!

Such a claim can be seen more clearly if we recast the effective hamiltonian by inverting the spherical coordinates to the (cartesian) components of the localized spins.

$$S_i^x = \cos \phi_i \sin \theta_i \quad S_i^y = \sin \phi_i \sin \theta_i \quad S_i^z = \cos \theta_i \quad (6.7)$$

Unfortunately, it turns out that the first order correction cannot be neatly inverted in this manner. However, such a structure does emerge at the second order correction which roughly has the following form:

$$\sum_{\dots} (\dots) \cdot \frac{|g_{i,j}^{\sigma, \sigma'}|^2}{E - E_0}$$

Below is the matrix of these mod squared values that have been inverted in terms of the cartesian spin components.

$$|g_{ij}^{\sigma, \sigma'}|^2 = \frac{t_{i,j}^2}{4} \begin{bmatrix} (1 + \vec{S}_i \cdot \vec{S}_j)^2 & 2(1 - (\vec{S}_i \cdot \vec{S}_j)^2) & (1 - \vec{S}_i \cdot \vec{S}_j)^2 \\ 2(1 - (\vec{S}_i \cdot \vec{S}_j)^2) & 4(\vec{S}_i \cdot \vec{S}_j)^2 & 2(1 - (\vec{S}_i \cdot \vec{S}_j)^2) \\ (1 - \vec{S}_i \cdot \vec{S}_j)^2 & 2(1 - (\vec{S}_i \cdot \vec{S}_j)^2) & (1 + \vec{S}_i \cdot \vec{S}_j)^2 \end{bmatrix} \quad (6.8)$$

We can clearly see a much nicer interpretation of the mediated interaction since these represent a simple heisenberg type coupling between the localized spins. However, we will not pursue the complete calculation since the leading order correction is non-zero.

Our treatment of the systems in this thesis so far have all been restricted at the mean-field level. While it is sufficient for qualitative results, it generates very poor quantitative estimates of phase boundaries. In some cases, it can result in entirely incorrect prediction of the existence of certain phases as well. As a result, we are motivated to look for better numerical techniques that can allow us to study the system beyond the mean-field level. In this chapter, we will discuss some of these techniques and the difficulties that arise due to the complexity involved in them.

7.1 Variational Monte Carlo

One of the issues with exact diagonalization is that the basis set scales exponentially with the system size. As a result, the memory required simply to represent the wavefunction on a computer quickly grows beyond bounds. This motivates us to look for ways to exploit structure in the wavefunction and find a more compact representation.

As a result, we try to leverage the variational principle and guess an ansatz for the wavefunction. The ground state is then obtained by tuning the free parameters to minimize the energy.

$$\Psi \equiv \Psi\{\alpha_i\}$$
$$\min_{\alpha_i} \langle \Psi\{\alpha_i\} | H | \Psi\{\alpha_i\} \rangle \geq E_0$$

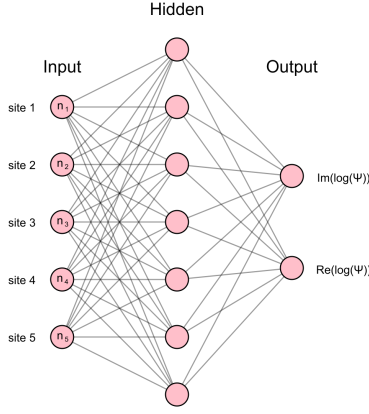


Figure 7.1: Pictorial representation of the neural network

However, the accuracy of the results strongly depend on how well the ansatz approximates the true wave-function. For example, the mean-field approach effectively introduces a site-decoupled ansatz which is a poor one as it ignores all long-range correlations. On the other hand, we have more sophisticated approaches like tensor networks and DMRG that exploit the entanglement structure to construct an ansatz.

We take a different approach here by utilizing a universal function approximator instead of any particular form of ansatz. In principle, a feed-forward neural network with sufficient hidden layers and nodes is capable of serving this purpose such that the variational parameters are simply the network weights. Let us now consider the wavefunction of the Bose-Hubbard model with N particles and M lattice sites in the occupation basis.

$$|\Psi\rangle = \sum_{\sum_i n_i = N} \psi(n_1, n_2, \dots, n_M) |n_1, n_2, \dots, n_M\rangle = \sum \psi(\mathbf{n}) |\mathbf{n}\rangle \quad (7.1)$$

The input layer of the network will have M nodes, such that the basis state $|\mathbf{n}\rangle \equiv |n_1, n_2, \dots, n_M\rangle$ can be set as an input as shown in Fig. 8.1. The values of the nodes on the hidden layers are computed as usual, using a hyperbolic tangent activation function:

$$u_j^{(0)} = n_j \quad ; u_m^{(i+1)} = \sum_{k=1}^{N_H^{(i)}} W_{mk}^{(i+1)} \tanh u_k^{(i)}(\mathbf{n}) + h_m^{(i+1)} \quad (7.2)$$

The output layer will have 2 nodes such that we can get the co-efficient of the input basis state like so:

$$\psi(\mathbf{n}) = \exp \left[u_1^{N_l}(\mathbf{n}) + i u_2^{N_l}(\mathbf{n}) \right] \quad (7.3)$$

The wavefunction can now be represented in this compact neural network once we tune the parameters, $\{W^{\mathbf{n}}, h^{\mathbf{n}}\}_1^{N_l}$ by minimizing the energy. Generally, the expectation value of

an operator, \hat{A} is calculated using the expression:

$$\langle A \rangle = \frac{\sum_{\mathbf{n}, \mathbf{n}'} \psi^*(\mathbf{n}) \langle \mathbf{n} | \hat{A} | \mathbf{n}' \rangle \psi(\mathbf{n}')}{\sum_{\mathbf{n}} |\psi(\mathbf{n})|^2} \quad (7.4)$$

However, if we compute every element of the sum by retrieving the coefficients from our neural network, we effectively lose the benefit of having a compact representation. Instead, we utilize the standard Monte Carlo scheme, where the basis states are importance sampled, using the Metropolis algorithm. Since our goal is to sample states $\{n\}$ following the distribution $|\psi(\mathbf{n})|^2 / \sum_{\mathbf{n}'} |\psi(\mathbf{n}')|^2$, we accept the proposal $\mathbf{n}_1 \rightarrow \mathbf{n}_2$ with probability $|\psi(\mathbf{n}_2)|^2 / |\psi(\mathbf{n}_1)|^2$ and compute the expectation value like so:

$$\left\langle \langle \mathbf{n} | \hat{H} | \mathbf{n} \rangle \frac{\psi(\mathbf{n}')}{\psi(\mathbf{n})} \right\rangle_M \equiv \langle H \rangle_M \quad (7.5)$$

where $\langle \dots \rangle_M$ indicates an average over the metropolis sampling of \mathbf{n} . Training the network weights to represent the wavefunction requires us to perform a gradient descent:

$$w \rightarrow w - \gamma \frac{\partial \langle \hat{H} \rangle_M}{\partial w} \quad (7.6)$$

where, γ is the learning rate, and the gradient can be computed using the following expression:

$$\frac{\partial \langle \hat{H} \rangle}{\partial w} \approx 2\text{Re}(\langle O_w \hat{H} \rangle_M - \langle O_w^* \rangle_M \langle \hat{H} \rangle_M) \quad O_w(\mathbf{n}) = \frac{1}{\psi(\mathbf{n})} \frac{\partial \psi(\mathbf{n})}{\partial w} \quad (7.7)$$

Details can be found in [ref]. Our implementation can be found on [github], however, in its current state it is unusable due to inefficient computation of the gradient. This leads to extremely large runtimes for even small system sizes. Further, a naive gradient descent approach gets trapped in local minima even for the Bose-Hubbard model. As a result, this line of exploration was not pursued further. It is worth noting, however, that there are larger and more mature projects that implement machine learning techniques to solve many body problems, such as NetKet.

7.2 Stochastic Series Expansion

We now turn to a class of extremely powerful methods that are broadly classified as Quantum Monte Carlo techniques. There are countless variations and flavors depending on the specifics of the system under consideration, but they all share the trait of utilizing Monte Carlo sampling in some capacity to solve quantum problems. We will focus on one flavor in particular, the stochastic series expansion (SSE).

Generally, the goal of such methods is to compute the partition function and hence the thermal expectation values of various observables of interest. We begin by performing

a Taylor expansion of the exponent around $\beta = 0$ and taking the trace with respect to an appropriate basis set $\{\alpha\}$.

$$Z = \text{Tr}\left\{e^{-\beta H}\right\} = \text{Tr}\left\{\sum_{n=0}^{\infty} \frac{(-\beta)^n}{n!} H^n\right\} = \sum_{\alpha} \sum_{n=0}^{\infty} \frac{(-\beta)^n}{n!} \langle \alpha | H^n | \alpha \rangle \quad (7.8)$$

We can view the above sum as a Monte Carlo sampling of the configurations, $(|\alpha\rangle, n)$ with the weight, $W(|\alpha\rangle, n) = \frac{(-\beta)^n}{n!} \langle \alpha | H^n | \alpha \rangle$. However, there is a glaring problem, that is the infinite sum over the expansion order, n . At first sight, such a situation seems impossible to deal with in a numerical algorithm. However, a solution presents itself if we analyze the nature of the energy and specific heat capacity calculated through this procedure.

$$\begin{aligned} \langle H \rangle &= \frac{1}{Z} \text{Tr}\left\{H e^{-\beta H}\right\} \\ &= \frac{1}{Z} \sum_{\alpha} \sum_{n=0}^{\infty} \frac{(-\beta)^n}{n!} \langle \alpha | H^{n+1} | \alpha \rangle \\ &= -\frac{1}{Z} \sum_{\alpha} \sum_{n=1}^{\infty} \frac{n}{\beta} \cdot \frac{(-\beta)^n}{n!} \langle \alpha | H^n | \alpha \rangle = \frac{\langle n \rangle}{\beta} \end{aligned} \quad (7.9)$$

Similarly, we get $\langle H^2 \rangle = \langle n(n-1) \rangle / \beta^2$. The expression for the specific heat can then be computed as follows.

$$C_v = \frac{\langle H^2 \rangle - \langle H \rangle^2}{T^2} = \langle n^2 \rangle - \langle n \rangle^2 - \langle n \rangle \quad (7.10)$$

Generally, the specific heat vanishes as $T \rightarrow 0$ for quantum systems, so we can write $\sigma_n = \langle n^2 \rangle - \langle n \rangle^2 = \langle n \rangle$. Thus, we have $\langle n \rangle \sim N\beta$ and $\sigma_n \sim \sqrt{N\beta}$ where N is the system size which is introduced since the energy roughly scales with the N . This tells us that the distribution of n that contributes to the sum is quite narrow and we can simply introduce a cut-off length L in our algorithm (that must be adjusted as the simulation progresses).

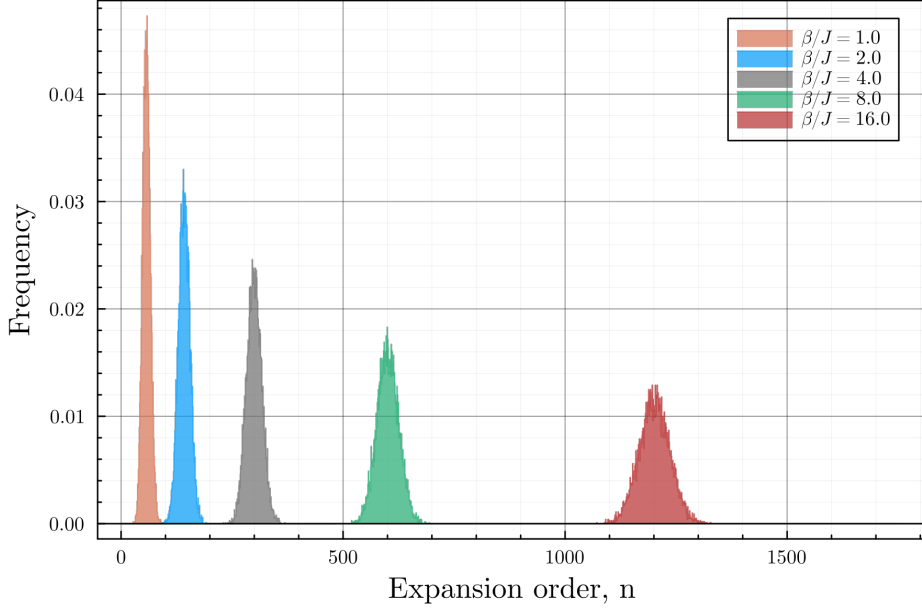


Figure 7.2: Distribution of expansion order in SSE

At this point, we note that computing the quantity $\langle \alpha | H | \alpha \rangle$ is generally non trivial, and so we introduce an important idea that makes the SSE tractable. Generally, lattice hamiltonians can be broken down as $H = -\sum_{a,b} H_{a,b}$, where b indicates the "bond" connecting two sites $i(b)$ and $j(b)$, and a indicates the class of the operator. Any power of the hamiltonian can then be written in terms of a sum over 'operator strings' $\{H_{ab}\}$.

$$(-H)^n = \sum_{\{H_{ab}\}} \prod_{p=1}^n H_{a(p),b(p)} \quad (7.11)$$

Putting this together with the fixed length scheme that was motivated above, we can write the partition function in the typical monte carlo format.

$$Z = \sum_{\alpha, H_{ab}} \frac{\beta^n (L-n)!}{L!} \langle \alpha | \prod_{p=1}^n H_{a(p),b(p)} | \alpha \rangle \quad \leftrightarrow \quad Z = \sum_{C_i} W(C_i) \quad (7.12)$$

$$\langle O \rangle = \frac{1}{Z} \sum_{\alpha, H_{ab}} \frac{\beta^n (L-n)!}{L!} \langle \alpha | O \prod_{p=1}^n H_{a(p),b(p)} | \alpha \rangle \quad \leftrightarrow \quad \langle A \rangle = \frac{\sum_{C_i} O(C_i) W(C_i)}{\sum_{C_i} W(C_i)} \quad (7.13)$$

We have now introduced an abstract configuration which is a 2-tuple consisting of $|\alpha\rangle$, an element of the basis set, and $\{H_{ab}\}$ which is a string of L bond operators. In order to work with the fixed-length scheme, we have also introduced $H_{0,0} = \mathbb{I}$ to pad the operator string, such that each string consists of n non-identity bond operators and $(L-n)$ identities, thus

sampling the expansion orders $n \in [1, L]$.

The problem has now reduced to ergodically sampling this configuration space according to their weights (which can be computed with ease due to the bond decomposition). An issue arises when the weights are not positive, in which case they cannot be interpreted as probabilities, thus giving rise to the infamous *sign problem*. This is usually the case for fermionic systems and systems with non-bipartite lattices geometries.

S=1/2 Heisenberg model

Let us now consider the spin-1/2 heisenberg model with anti-ferromagnetic interactions ($J > 0$) on a square lattice. We choose this particular example since it is quite illustrative of the SSE technique while also having some relevance to the Bose-Hubbard model that we will discuss at the end of the chapter.

$$H = J \sum_{\langle i,j \rangle} S_i \cdot S_j \quad (7.14)$$

A natural basis set to use in our expansion is the S_z -basis, $|S_1^z, S_2^z, \dots, S_N^z\rangle$. We can now rewrite the hamiltonian as a sum of bond operators:

$$H_{1,b} = \frac{1}{4} - S_{i(b)}^z S_{j(b)}^z \quad H_{2,b} = \frac{1}{2}(S_{i(b)}^+ S_{j(b)}^- + S_{i(b)}^- S_{j(b)}^+) \quad (7.15)$$

$$H = J \sum_{b=1}^B [S_{i(b)}^z S_{j(b)}^z + \frac{1}{2}(S_{i(b)}^+ S_{j(b)}^- + S_{i(b)}^- S_{j(b)}^+)] = -J \sum_{b=1}^{N_B} (H_{1,b} - H_{2,b}) + \frac{J N_b}{4} \quad (7.16)$$

Here, we have introduced two 'classes' of bond operators, that is, those that are diagonal ($H_{1,b}$) and off-diagonal ($H_{2,b}$) in the S_z -basis. There is also an important restriction on the choice of the bond operators $H_{a,b}$, namely, that they must be non-branching, i.e, $H_{a,b} |\alpha_i\rangle = C_{a,b}^{i,j} |\alpha_j\rangle$ where $|\alpha_i\rangle$ and $|\alpha_j\rangle$ are single elements of the chosen basis set. This implies that each configuration can equivalently be understood as a periodic sequence of basis elements (due to the cyclic nature of the trace).

$$C \equiv |\alpha_0\rangle \rightarrow |\alpha_1\rangle \rightarrow \dots \rightarrow |\alpha_{L-1}\rangle \rightarrow |\alpha_0\rangle \quad |\alpha_i\rangle = \prod_{p=1}^i H_{a(p),b(p)} |\alpha_0\rangle \quad (7.17)$$

Notice that we have also introduced a constant energy shift in order to force the matrix elements, and hence the configuration weights to be positive. Since the bond operators only act on two sites, we can list out all of these matrix elements:

$$\begin{aligned} \langle \uparrow_{i(b)} \downarrow_{j(b)} | H_{1,b} | \uparrow_{i(b)} \downarrow_{j(b)} \rangle &= \frac{1}{2} & \langle \downarrow_{i(b)} \uparrow_{j(b)} | H_{2,b} | \uparrow_{i(b)} \downarrow_{j(b)} \rangle &= \frac{1}{2} \\ \langle \downarrow_{i(b)} \uparrow_{j(b)} | H_{1,b} | \downarrow_{i(b)} \uparrow_{j(b)} \rangle &= \frac{1}{2} & \langle \uparrow_{i(b)} \downarrow_{j(b)} | H_{2,b} | \downarrow_{i(b)} \uparrow_{j(b)} \rangle &= \frac{1}{2} \end{aligned}$$

Note that any bond operator can only act on anti-parallel spins, since all other configurations have a vanishing matrix element. Further, we see that not only are the non-zero matrix elements positive but they are also equal. This greatly simplifies the algorithm, since the weight of any valid configuration is simply computed as follows.

$$W(\alpha, \{H_{a,b}\}) = \left(\frac{\beta}{2}\right)^n \frac{(L-n)!}{L!} \quad (7.18)$$

The challenge now is to come up with a sampling scheme that generates operator strings that samples such periodic sequences of basis elements. There are usually three types of updates that are required to maintain ergodicity:

- **Diagonal update:** This changes n , the number of non-identity bond operators in the operator string. Such an update simply replaces an identity operator with a diagonal one (or vice versa) if the spin states it acts on is anti-parallel.
- **Off-diagonal update:** Off-diagonal operators cannot be added or removed individually as was the case with the diagonal operators, since the periodicity of the basis state has to be preserved. As a result, one has to manipulate pairs of off-diagonal operators acting on the same sites, however such an update scheme is quite inefficient. Instead, another approach known as the loop operator update is used wherein a loop is constructed across the entire configuration, connecting the spin sites at the base of several operators, which are then flipped simultaneously in an analogous manner to the cluster updates in the ising model.
- **Spin-flip update:** Finally, if a particular spin is not acted upon by any operators, it can be flipped to sample a different basis state $|\alpha\rangle$. However, this update is not strictly required nor efficient since the off-diagonal updates already sample the basis states as well.

The probability of accepting these updates can be computed quite directly by means of the usual metropolis technique:

$$P_{\text{accept}}(A \rightarrow B) = \min \left(\frac{W(B)P_{\text{select}}(B \rightarrow A)}{W(A)P_{\text{select}}(A \rightarrow B)}, 1 \right) \quad (7.19)$$

We will not cover these in detail here as this chapter is mostly meant to give an introduction to the basic idea of quantum monte carlo techniques. The interested reader may find these details as well as an ingenious way to visualize and implement the SSE in Sandvik's paper.

Once we are able to sample the configurations ergodically, diagonal observables can be computed easily as they do not alter the sequence of basis states. On the other hand, off-diagonal observables in general are quite hard to compute. However, any off-diagonal operator, $H_{2,b}$, which is a part of the hamiltonian itself is found to be related to the expectation value of the number of occurrences of the operator in the operator string. For example, this is what we found for the energy $\langle H \rangle = -\langle n \rangle / \beta$. Luckily, most of the observables that are useful for our purposes fall within these two categories.

Results

We have performed the SSE for various lattice sizes and temperatures, recording $n = 10000$ samples for computing each quantity. The results are shown as in Fig. 8.3. Although there are strong finite-size effects in most of the plots, we can see for $L = 48$ that the (staggered) magnetization does indeed undergo a transition somewhere between $J \cdot T \in [0.2, 0.6]$ indicating a shift from the anti-ferromagnetic state to a paramagnet. Peculiarly, the magnetic susceptibility χ seems to also have a continuous transition around the same region instead of a divergence as expected from a second order transition. On the other hand, we have some hint of divergence from the specific heat plot around $J \cdot T \approx 0.6$.

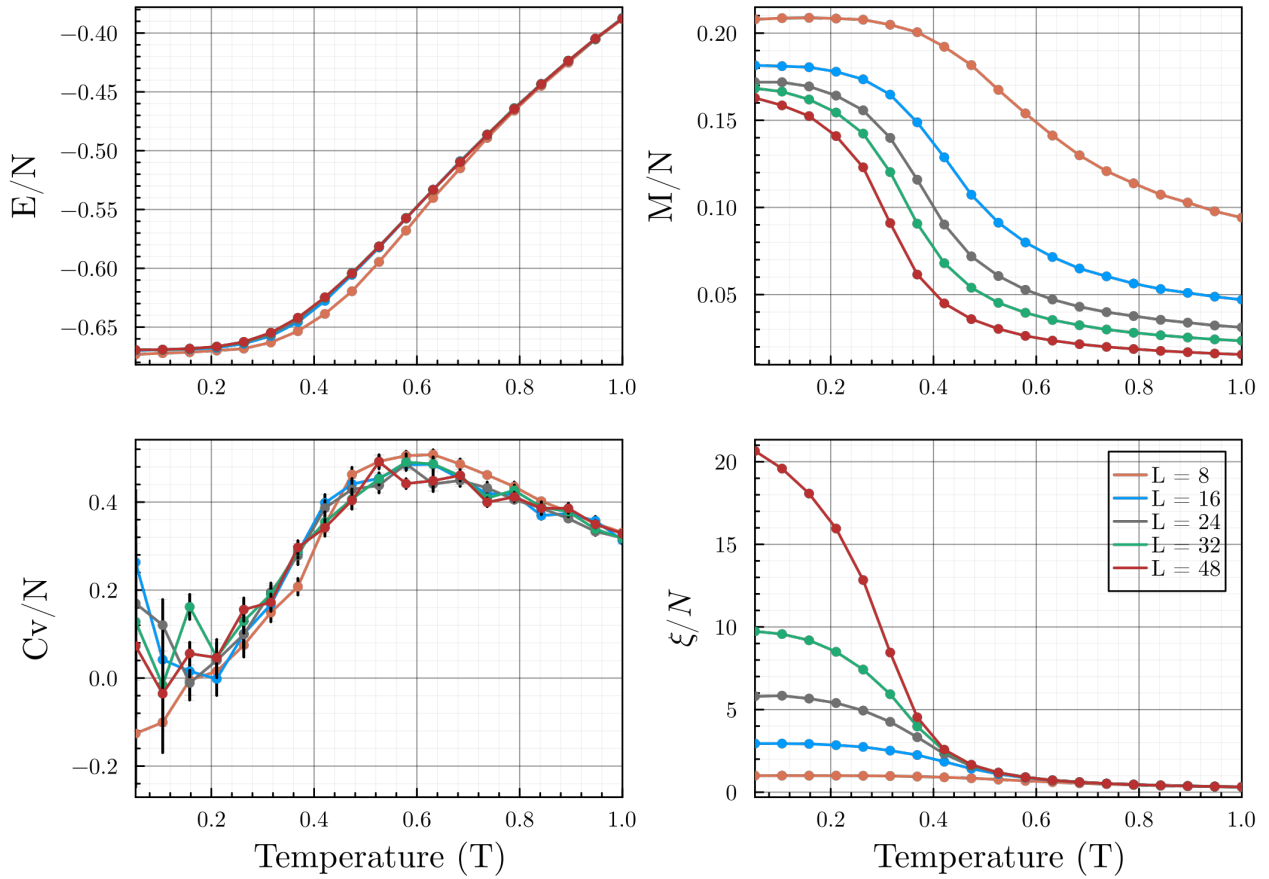


Figure 7.3: Tracking various quantities calculated using SSE

In order to extract a better estimate of the critical temperature by dealing with the finite size effects, we calculate the Binder cumulant for various lattice sizes in Fig. 8.4.

$$U_L = 1 - \frac{\langle M^4 \rangle_L}{3 \langle M^2 \rangle_L^2} \quad (7.20)$$

We see that the curves roughly intersect at $J \cdot T \approx 0.22$. As it stands, these results significantly contradict with each other and we have not been able to resolve this so far.

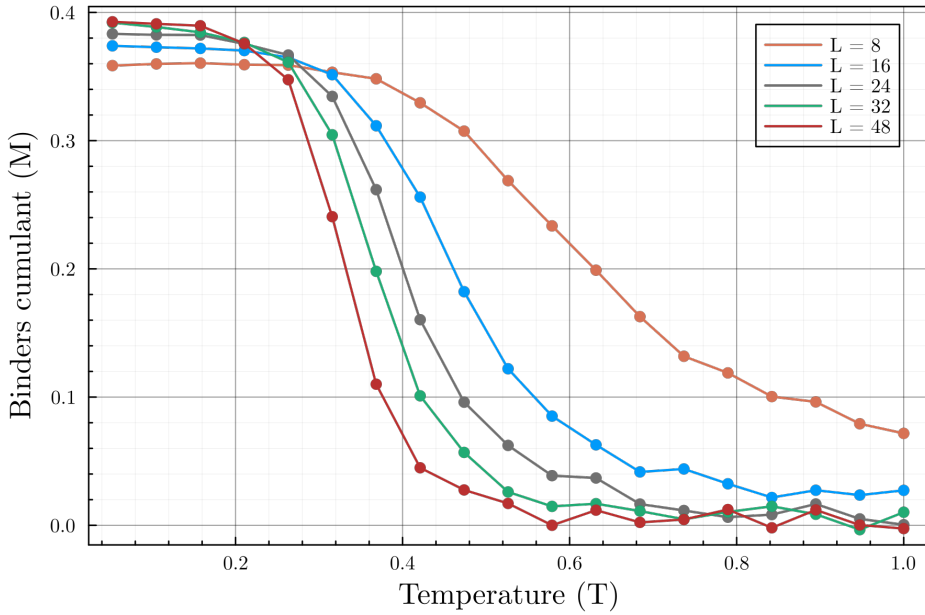


Figure 7.4: Binder cumulant

Mapping to bosons

The discussion so far seems rather unrelated to the rest of the thesis, however, a closer look at the heisenberg hamiltonian reveals that this is not the case:

$$H = J \sum_{\langle i,j \rangle} \vec{S}_i \cdot \vec{S}_j = J \sum_{\langle i,j \rangle} \left[\frac{1}{2} (S_i^+ S_j^- + S_i^- S_j^+) + S_i^z S_j^z \right] \quad (7.21)$$

Consider the mapping $S_i^+ \rightarrow a_i^\dagger$, $S_i^- \rightarrow a_i$ and $S_i^z = n_i - 1/2$. The hamiltonian is then oddly reminiscent of the extended bose-hubbard model.

$$H = \frac{J}{2} \sum_{\langle i,j \rangle} (a_i^\dagger a_j + a_j^\dagger a_i) + J \sum_{\langle i,j \rangle} n_i n_j \quad (7.22)$$

where $t = -J/2$ and $V = J$. Note that the on-site interaction term is missing. This is because we have effectively mapped classical spin-1/2 particles to *hardcore* bosons, i.e, in the limit of $U \rightarrow \infty$ s.t. $\langle n_i \rangle \in \{0,1\}$. Loosely we can think of states having $\langle S^z \rangle = -1/2$ and $\langle S^z \rangle = 1/2$ corresponding to $\langle n \rangle = 0$ and $\langle n \rangle = 1$ boson occupation, respectively. Note that the a^\dagger (a) operators here are not general boson operators, but specifically ones that create (annihilate) hard-core bosons.

In the most general case, we can map a spin-S anisotropic XXZ model to a semi-hardcore extended bose hubbard model with maximum occupation of $2S$:

$$\begin{aligned}
H &= J_x \sum_{\langle i,j \rangle} (S_i^+ S_j^- + S_i^- S_j^+) + J_z \sum_{\langle i,j \rangle} S_i^z S_j^z + h_z \sum_i S_i^z & t &\equiv J_x \\
H &= -t \sum_{\langle i,j \rangle} (a_i^\dagger a_j + a_j^\dagger a_i) + V \sum_{\langle i,j \rangle} n_i n_j - \mu \sum_i n_i & V &\equiv J_z \\
&&&\mu \equiv J_z - h_z
\end{aligned}$$

However, in such a case, there are many more non-zero matrix elements that exist which are also not necessarily equal in magnitude. As a result, the operator loop update has to be redesigned since there is no unique deterministic loop that can be constructed for a given configuration. This resulted in the formulation of the directed loop algorithm which applies to the most general situations.

Our implementation of the SSE for the isotropic spin-1/2 heisenberg model can be found here. Although we intended to implement the directed loop algorithm as well, we were unable to do so within the constraint of the thesis and will not discuss its details here.

7.2.1 Path integral QMC

While the SSE is quite straightforward conceptually, it can efficiently generate samples only when the diagonal and off-diagonal terms are of comparable magnitude ($t \sim U, t \sim V$ for e.g.). This is generally satisfied for spin systems, however the interesting regions in bosonic systems occur for $t \ll U, t \ll V$. As a result, the SSE sampling scheme is not the best choice for our purposes. Instead, we turn to a related class of algorithms loosely termed as path integral QMC. We first discuss the discrete formulation.

$$Z = \text{Tr}\left\{e^{-\beta H}\right\} = \text{Tr}\left\{\prod_{l=1}^L e^{-\Delta\tau H}\right\} \quad \Delta\tau = \beta/L \quad (7.23)$$

Instead of taylor expanding the exponential, we utilize a trotter decomposition to cast the sum in terms of the usual monte carlo language by inserting completeness relations of our preferred basis set, $\{\alpha\}$. We then have:

$$Z = \sum_{\alpha_0} \sum_{\alpha_1} \cdots \sum_{\alpha_{L-1}} \langle \alpha_0 | e^{-\Delta\tau H} | \alpha_{L-1} \rangle \dots \langle \alpha_2 | e^{-\Delta\tau H} | \alpha_1 \rangle \langle \alpha_1 | e^{-\Delta\tau H} | \alpha_0 \rangle \quad (7.24)$$

$$Z \approx \sum_{\{\alpha\}} \langle \alpha_0 | 1 - \Delta\tau H | \alpha_{L-1} \rangle \dots \langle \alpha_2 | 1 - \Delta\tau H | \alpha_1 \rangle \langle \alpha_1 | 1 - \Delta\tau H | \alpha_0 \rangle \quad (7.25)$$

where, the error falls off as $\mathcal{O}(\Delta\tau)$ and vanishes in the limit $\Delta\tau \rightarrow 0$. The configurations here are quite similar to the idea we introduced in the SSE involving a cyclic sequence of basis states. While the diagonal parts of H leave the basis state unaltered, the off-diagonal ones do not. Effectively, we can view this procedure as having introduced a new dimension, $\Delta\tau$ to our system.

In principle, since the results of the above method are only exact when $\Delta\tau \rightarrow 0$, one can perform the simulation for various values of $\Delta\tau$ and extrapolate them to get the exact

results. However, it turns out that such a technique is unnecessary as we can, in fact, take the limit exactly to formulate a continuous time path integral approach.

$$Z = \text{Tr} \left\{ e^{-\beta H} \right\} = \text{Tr} \left\{ \mathcal{T} e^{\beta H_0} \exp \left\{ - \int_0^\beta d\tau V(\tau) \right\} \right\} \quad (7.26)$$

where, $V(\tau) = e^{\tau H_0} V e^{-\tau H_0}$. The exponential can be expanded iteratively like so:

$$Z = \text{Tr} \left\{ e^{-\beta H_0} \sum_{n=0}^{\infty} \int_0^\beta d\tau_1 \int_0^{\tau_1} d\tau_2 \cdots \int_0^{\tau_{n-1}} V(\tau_1) \dots V(\tau_n) \right\} \quad (7.27)$$

By inserting basis sets between the elements, this formulation becomes quite similar to the discrete case, except that the $d\tau$ dimension is now continuous. However, a naive sampling of these configurations would result in critical slowing down near the phase boundaries. There exists an analog of the directed loop updates for the SSE for sampling configurations in the path integral approach, called the worm algorithm which solves this issue. We intend to utilize this technique in our future studies of the system to obtain more quantitative results.